Available online at www.sciencedirect.com
SCIENCE DIRECT®
ELSEVIER
International Journal of Solids and Structures 43 (2006) 3569–3595
INTERNATIONAL JOURNAL OF SOLIDS and STRUCTURES
www.elsevier.com/locate/ijsolstr

Micro-mechanical investigation of material instability in granular assemblies

François Nicot [a,*,1], Félix Darve [b,1]

[a] *Cemagref, Unité de Recherche Erosion Torrentielle Neige et Avalanches, Domaine Universitaire BP 76, 38402 Saint Martin d Heres, Grenoble, France*
[b] *Laboratoire Sols Solides Structures, UJF-INPG-CNRS, Grenoble, France*

Received 2 March 2005; received in revised form 6 July 2005
Available online 21 September 2005

Abstract

It is now well established that for non-associated materials such as geomaterials, there exists a wide domain strictly within the plastic limit where different failure modes can coexist. In particular, material instability in the sense given by Hill, related to the vanishing of the second-order work, can potentially occur. In this paper we examine the occurrence of such instabilities from the simulation of drained triaxial paths, followed by the computation of two-dimensional, then fully three-dimensional Gudehus response-envelopes using the micro-directional model. This model can be seen in the continuity of Hill's multi-slip theory, because it accounts for the association of a large number of elementary elasto-plastic bodies. Each body is linked to a contact direction in physical space and therefore takes into account the behavior of the contacts oriented along that direction. Simulations confirmed that some loading directions led to the vanishing of the second-order work. In line with the research initiated by Mandel, a micro-mechanical analysis of the origin of these potential instabilities revealed that this macro-scale phenomenon could be directly related to the constitutive nature of the local contact model between neighboring particles. Finally, this investigation provides a clear physical understanding of Hill's material stability condition for frictional materials.

Keywords: Homogenization; Granular material; Hill's material stability; Love formula; Micro-structure; Multi-scale modeling; Second-order work

* Corresponding author. Tel.: +33 4 76 76 27 70; fax: +33 4 76 51 38 03.
E-mail address: francois.nicot@grenoble.cemagref.fr (F. Nicot).
[1] RNVO Research Group (“Natural Hazards and Structure Vulnerability”).

0020-7683/$ - see front matter © 2005 Elsevier Ltd. All rights reserved.
doi:10.1016/j.ijsolstr.2005.07.008

1. Introduction

In the framework of continuum mechanics, Hill's material instability criterion applies to conjugate macroscopic variables, namely $\mathrm{d}\overline{\overline{\sigma}}$ and $\mathrm{d}\overline{\overline{\varepsilon}}$, which are related by constitutive equations (Hill, 1958). This criterion, applied to a material point, states that for a given material after a given stress–strain history, this material point is reputed to be unstable if at least one stress increment $\mathrm{d}\overline{\overline{\sigma}}$ exists, associated with a strain response $\mathrm{d}\overline{\overline{\varepsilon}}$, so that $\mathrm{d}^2W = \mathrm{d}\overline{\overline{\sigma}} : \mathrm{d}\overline{\overline{\varepsilon}} \leqslant 0$.

Various bifurcations and their related failure modes coexist in granular materials, essentially because they are characterized by strongly non-associated plastic strains. These failure modes are described by different criteria:

$\det \overline{\overline{N}} = 0$	(the plastic limit condition, with $\mathrm{d}\sigma_\alpha = N_{\alpha\beta}\mathrm{d}\varepsilon_\beta$, $\alpha, \beta = 1, \ldots, 6$)
$\det \vec{n}\overline{\overline{L}}\vec{n} = 0$	(the localization condition, with $\mathrm{d}\sigma_{ij} = L_{ijkl}\mathrm{d}\varepsilon_{kl}$, $i, j, k, l = 1, 2, 3$)
$\mathrm{d}^2W = \mathrm{d}\overline{\overline{\sigma}} : \mathrm{d}\overline{\overline{\varepsilon}} \leqslant 0$	(the necessary instability condition; Hill, 1958)

If flutter instabilities are excluded, it has been proven (Nova, 1994; Bigoni and Hueckel, 1991) that this last condition is the "first" to be met along a loading path from an isotropic initial state. The proof is essentially based on the fact that Hill's condition is equivalent to the vanishing value of the determinant of the symmetric part of $\overline{\overline{N}}$ for the simplest elasto-plastic relations. Moreover, it seems that the second-order work condition is linked to diffuse modes of failure (Darve et al., 2004).

Thus, to deepen the analysis by the micro-directional model, one should investigate the variations of the macroscopic second-order work as a function of strain probe direction, since d^2W is essentially a directional quantity. Indeed, with $\mathrm{d}\overline{\overline{\sigma}} = \overline{\overline{N}}(\overline{\overline{v}})\mathrm{d}\overline{\overline{\varepsilon}}(\overline{\overline{v}} = \mathrm{d}\overline{\overline{\varepsilon}}/\|\mathrm{d}\varepsilon\|)$, $\mathrm{d}^2W = \mathrm{d}\overline{\overline{\sigma}} : \mathrm{d}\overline{\overline{\varepsilon}} = {}^t\overline{\overline{\varepsilon}}\,\overline{\overline{N}}(\overline{\overline{v}})\mathrm{d}\overline{\overline{\varepsilon}}$ and $\frac{\mathrm{d}^2W}{\|\mathrm{d}\overline{\overline{\varepsilon}}\|^2} = {}^t\overline{\overline{v}}\,\overline{\overline{N}}(\overline{\overline{v}})\overline{\overline{v}}$ are successively produced. In particular, it is of great interest to verify whether the second-order work vanishes for certain strain probe directions, since this is a proof of material instability (Hill, 1958). In this case, failure (or strain uncontrollability, in the sense defined by Nova, 1994) may occur during loading within the plastic limit (Bigoni and Hueckel, 1991). This approach for investigating the general notion of failure in granular geomaterials seems to be particularly promising and could provide valuable elements to explain and (in the future) to predict catastrophic phenomena such as rockfalls or landslides (Darve and Laouafa, 2000, 2002; Laouafa and Darve, 2002; see an overview in Darve and Vardoulakis, 2005).

In the first part of the paper, we will outline the micro-directional model. For a complete and meticulous presentation, the reader can refer to Nicot (2003a), Nicot and Darve (2004, 2005). The model proposed belongs within the general framework of multi-scale approaches based on analyses on two different scales. On a small scale, the properties of the materials, whose internal length corresponds to the size of the particles considered as rigid bodies, will be described in simple terms (Mehrabadi and Cowin, 1978; Nemat-Nasser et al., 1981; Nemat-Nasser and Mehrabadi, 1983; Christoffersen et al., 1981; Kanatani, 1983, 1984; Satake, 1978, 1982; Chang, 1992; Chang and Liao, 1994). Complexity will appear on larger scales (macroscopic scales), because purely geometrical nonlinear effects occur inside a large number of particles. The constitutive behavior of a granular assembly is derived by taking a statistical description of the fabrics into account. The location of each particle is ignored, but the probability that some contacts exist in a given direction is investigated. Modeling the creation or the loss of contacts in given directions makes it possible to analyze how the probability density of having contacts in these directions evolves. These different aspects have been considered and discussed in the past (Nemat-Nasser and Mehrabadi, 1984; Mehrabadi et al., 1993; Balendran and Nemat-Nasser, 1993a,b; Nemat-Nasser, 2000; Nemat-Nasser and Zhang, 2002).

The second part of the paper investigates material stability, in the sense given by Hill, 1958. The existence of unstable loading directions is verified from the computation of Gudehus' response-envelopes (Gudehus, 1979) in two-dimensional and three-dimensional conditions. Finally, a micro-mechanical interpretation of

this outstanding aspect is attempted, highlighting the fundamental role played by the contact model introduced, which can be regarded as the basic element of any particle assembly.

2. The micro-directional model

In light of a general review of the literature dealing with the mechanical behavior of granular media, the reader may be puzzled by the considerable number of constitutive models currently in use. Furthermore, these models often differ, notably in their basic approach. Ignoring rate-dependent models, examples include associate or non-associate elasto-plastic theories (see for example Taylor, 1934, 1938; Drucker and Prager, 1952; Hill, 1967a; Rice, 1970, 1975), generalized plasticity (Zienkiewicz and Mroz, 1984; Pastor et al., 1990), endochronic models (Bazant, 1978), hypoplastic theories (Kolymbas, 1991, 1999), and incrementally nonlinear models (Darve, 1990; Darve et al., 1995). These approaches can be ranged in the category of phenomenological approaches, to the extent that they directly formulate the observed phenomena in an appropriate and sometimes sophisticated mathematical formalism. They differ basically from multi-scale approaches, which attempt to analyze and derive macroscopic properties from a local description of the medium. Such approaches can make use of homogenization techniques; an abundant literature deals with this subject, and we mention here only a few pioneering contributions: De Josselin de Jong, 1959, 1971; Spencer, 1964; Mehrabadi and Cowin, 1978; Nemat-Nasser et al., 1981; Nemat-Nasser and Mehrabadi, 1983; Christoffersen et al., 1981; Kanatani, 1983, 1984; Satake, 1978, 1982; Chang, 1992; Chang and Liao, 1994; Cambou, 1993; Cambou et al., 1995. Other methods take advantage of numerical modeling such as the discrete element method (Cundall and Strack, 1979; Kishino, 1988; Cundall and Roger, 1992; Bardet and Proubet, 1989; Bardet, 1994a, and more recently Calvetti et al., 2003; Kishino, 2003). The term "multi-scale" means that this range of methods was developed to account for the micro-structure of granular media.

The micro-directional model belongs to the class of multi-scale approaches and was initially developed to describe the behavior of snow, modeled as an assembly of ice particles (Nicot, 2003b, 2004). Fundamentally, this model is based on a homogenization procedure within a representative volume element (RVE), which is assumed to contain a "sufficient" number of spherical grains (or contacts). In this approach, the location of each grain is ignored and only contact directions are accounted for; the probability that some contacts exist in a given direction is investigated and local variables are averaged in each direction of the physical space, so that directional local variables are introduced. The homogenization procedure can be resolved in three stages (Fig. 1): first, a kinematic localization procedure assesses the directional average displacement field $\mathrm{d}\widehat{\vec{u}}$ in terms of the macroscopic strain tensor $\mathrm{d}\overline{\overline{\varepsilon}}$; then, local constitutive equations are introduced to relate both kinematic and static directional average variables; and finally a static averaging procedure is built to infer the macroscopic stress tensor $\mathrm{d}\overline{\overline{\sigma}}$ from the distribution of directional average forces $\mathrm{d}\vec{F}$ between neighboring particles in contact. The complex macroscopic behavior comes from the multiplicity of intergranular contacts in various mechanical states (from elasticity to plasticity).

These different steps have been considered and discussed by a number of authors (Nemat-Nasser and Mehrabadi, 1984; Jenkins and Strack, 1993; Mehrabadi et al., 1993; Balendran and Nemat-Nasser,

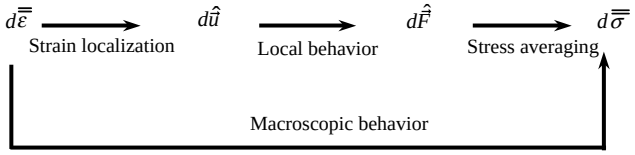

Fig. 1. General homogenization scheme relating the stress tensor and the strain tensor.

1993a,b; Nemat-Nasser, 2000; Nemat-Nasser and Zhang, 2002). In its fundamentals, this kind of model can be regarded as an association of multiple elastic–plastic bodies; each body, related to a given contact direction, takes into account the behavior of contacts in this direction. Note that this approach is within the continuity of Hill's multislip theory (Hill, 1965, 1966, 1967b); for a certain class of materials such as metals, which can be considered as a set of element crystals, preferential sliding directions exist. Hill's multislip theory is a general type of cross-coupling between glide and hardening on different slip systems. The theory of microplane models (Zienkiewicz and Pande, 1977; Bazant and Gambarova, 1984) and the generalized plasticity with multiple plastic mechanisms (Pastor et al., 1990) are typical examples of the multislip theory. In such cases, there are several linear relations between $\mathrm{d}\overline{\overline{\varepsilon}}$ and $\mathrm{d}\overline{\overline{\sigma}}$, which means that in the incremental loading space there are several domains where the incremental constitutive relation is linear. These domains, which are hypercones in the six-dimensional incremental loading space, have been called tensorial zones (Darve and Labanieh, 1982; Darve et al., 1995). The constitutive relation can be characterized as being incrementally piece-wise linear. For granular materials, there is no preferential sliding direction. In the plastic regime, the constitutive tensor no longer varies in a discontinuous manner with the incremental loading direction, changing from one value in a given tensorial zone to another value. On the contrary, the directional variation of the constitutive tensor is continuous and the class of incrementally nonlinear constitutive relations is obtained (Darve, 1990). From a mathematical point of view, the constitutive relation does not exhibit the same structure in both cases. The incremental relation of rate-independent materials can be expressed in a general manner by $\mathrm{d}\overline{\overline{\sigma}} = F_h(\mathrm{d}\overline{\overline{\varepsilon}})$, where h represents the state variables and the memory parameters characterizing the previous strain–stress history. Because of the rate-independency condition, F is a homogeneous function of degree one and Euler's identity implies:

$$\mathrm{d}\overline{\overline{\sigma}} = \frac{\partial F}{\partial(\mathrm{d}\overline{\overline{\varepsilon}})}\mathrm{d}\overline{\overline{\varepsilon}} = \overline{\overline{N}}_h(\overline{\overline{v}})\,\mathrm{d}\overline{\overline{\varepsilon}} \tag{1}$$

with $\overline{\overline{v}} = \dfrac{\mathrm{d}\overline{\overline{\varepsilon}}}{\|\mathrm{d}\varepsilon\|}$. Constitutive tensor $\overline{\overline{N}}$ is the gradient of the tensorial function F. For incrementally piecewise linear relations, $\overline{\overline{N}}$ varies in a discontinuous manner with respect to $\overline{\overline{v}}$, whereas for incrementally nonlinear relations the variation is continuous.

2.1. The macroscopic stress tensor

Considering a representative volume element located around a given material point M, the macroscopic stress tensor $\overline{\overline{\sigma}}$ is computed from the local contact forces $\vec{F}^c$ between each pair of particles in contact in the RVE. The averaging procedure necessary to go from the local intergranular forces to the stress tensor has been largely discussed (Love, 1927; Weber, 1966; Christoffersen et al., 1981; Mehrabadi et al., 1982; Cailleerie, 1995), and now it seems well established that $\overline{\overline{\sigma}}$ and $\vec{F}^c$ can be related by the Love formula of homogenization:

$$\sigma_{ij} = \frac{1}{v_e}\sum_c F_i^c l_j^c \tag{2}$$

where F_i^c is the ith component of the contact force $\vec{F}^c$, l_j^c is the jth component of the branch vector $\vec{l}^c$ joining the centers of particles in contact on contact c, and the sum is extended to all the contacts occurring in volume v_e.

Eq. (2) is expressed under a discrete formalism, but it can be extended to a continuum formalism by integrating over all the contact directions $\vec{n}(\theta,\varphi) = \cos\varphi\vec{x}_1 + \sin\varphi\cos\theta\vec{x}_2 + \sin\varphi\sin\theta\vec{x}_3$, where $(\vec{x}_1,\vec{x}_2,\vec{x}_3)$ constitutes a direct Cartesian frame of the physical space, and both θ and φ are continuous variables in $[0;\pi]$ (Fig. 2).

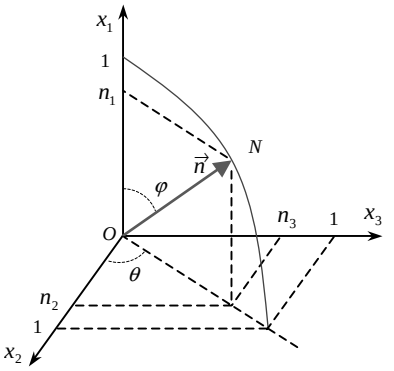

Fig. 2. Continuous description of the normal direction of contact.

Defining $\omega_e(\theta,\varphi) = \omega(\theta,\varphi)v_e$ the number of contacts oriented along a given direction, it follows (Nicot and Darve, 2004, 2005) that:

$$\sigma_{ij} = \int\int_{[o;\pi]^2} 2r_g\omega(\theta,\varphi)\widehat{F}_i(\theta,\varphi)n_j(\theta,\varphi)\sin\varphi\,\mathrm{d}\theta\,\mathrm{d}\varphi \tag{3}$$

where r_g denotes the mean radius of the sphere-shaped grains and $\widehat{\vec{F}}$ is the average of all contact forces $\vec{F}^c$ associated with contacts oriented in the direction $\vec{n}$.

2.2. The strain localization relation

The localization method for deducing a local displacement field from the strain tensor is more controversial and the solution, in principle, is not unique. The strain localization operator is inferred from the assessment of the strain energy increment, on the one hand from macroscopic variables $(\overline{\overline{\sigma}}, \mathrm{d}\overline{\overline{\varepsilon}})$, and on the other hand from the average local variables $(\widehat{\vec{F}}(\theta,\varphi), \mathrm{d}\widehat{\vec{u}}(\theta,\varphi))$, where $\widehat{\vec{u}}(\theta,\varphi)$ is the directional kinematic variable linked to $\widehat{\vec{F}}(\theta,\varphi)$. Thus, if the representative volume element is macro-homogeneous (at the sense given by Hill, 1967c), it can be shown that the kinematic average local field can be deduced from the macroscopic strain tensor as follows (Nicot and Darve, 2004, 2005):

$$\mathrm{d}\widehat{u}_i(\theta,\varphi) = 2r_g\mathrm{d}\varepsilon_{ij}n_j(\theta,\varphi) \tag{4}$$

2.3. Local constitutive relations

The local behavior is described properly using a contact mechanical model relating both the local normal force F_c^n and the local tangential force F_c^t to both the local normal relative displacement u_c^n and the local tangential relative displacement u_c^t. Many models have been proposed in the literature (Bardet, 1998), the simplest one being the elastic–plastic model, which introduces a normal elastic stiffness k_n and a tangential elastic stiffness k_t, both constant, and a local friction angle φ_g.

In order to define a local stiffness matrix, it is useful to introduce a local unit vector frame $\{\vec{n},\vec{t}_1,\vec{t}_2\}$, where $\vec{n}$ is the vector perpendicular to the contact plane, $\vec{t}_1 = \dfrac{\vec{F}_t}{\|\vec{F}_t\|}$ and $\vec{t}_2 = \vec{n}\wedge\vec{t}_1$ (Fig. 3).

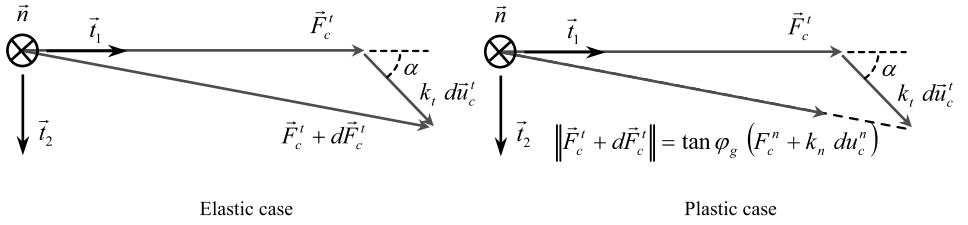

Fig. 3. Definition of the local vector frame.

In these conditions, the following local constitutive incremental relations can be inferred:

$$\mathrm{d}F_c^{\mathrm{n}} = k_n\,\mathrm{d}u_c^{\mathrm{n}} \tag{5a}$$

$$\mathrm{d}\vec{F}_c^{\mathrm{t}} = \min\{\|\vec{F}_c^{\mathrm{t}} + k_t\mathrm{d}\vec{u}_c^{\mathrm{t}}\|, \tan\varphi_{\mathrm{g}}(F_c^{\mathrm{n}} + k_n\,\mathrm{d}u_c^{\mathrm{n}})\}\frac{\vec{F}_c^{\mathrm{t}} + k_t\,\mathrm{d}\vec{u}_c^{\mathrm{t}}}{\|\vec{F}_c^{\mathrm{t}} + k_t\,\mathrm{d}\vec{u}_c^{\mathrm{t}}\|} - \vec{F}_c^{\mathrm{t}} \tag{5b}$$

Furthermore, granular assemblies are not able to sustain local tensile stress. This is a fundamental feature of this type of material. The following condition is therefore added:

$$F_c^{\mathrm{n}} > 0 \tag{6}$$

It will be assumed hereafter that Eqs. (5) and (6) also apply to the directional average variables $\widehat{\vec{u}}(\theta,\varphi)$ and $\widehat{\vec{F}}(\theta,\varphi)$.

In the $(\vec{n},\vec{t}_1,\vec{t}_2)$ frame, $\mathrm{d}\widehat{\vec{F}} = \mathrm{d}\widehat{F}_n\vec{n} + \mathrm{d}\widehat{F}_{t_1}\vec{t}_1 + \mathrm{d}\widehat{F}_{t_2}\vec{t}_2$ and $\mathrm{d}\widehat{\vec{u}} = \mathrm{d}\widehat{u}_n\vec{n} + \mathrm{d}\widehat{u}_{t_1}\vec{t}_1 + \mathrm{d}\widehat{u}_{t_2}\vec{t}_2$. Introducing the stiffness matrix $\widehat{K}$ as $\mathrm{d}\widehat{\vec{F}} = \widehat{K}\,\mathrm{d}\widehat{\vec{u}}$, we can note (see Appendix A) that in elastic conditions, the stiffness matrix $\widehat{K}^e$ is expressed in the $(\vec{n},\vec{t}_1,\vec{t}_2)$ frame as:

$$\widehat{K}^e = \begin{vmatrix} k_n & 0 & 0 \\ 0 & k_t & 0 \\ 0 & 0 & k_t \end{vmatrix} \tag{7}$$

whereas in plastic conditions, omitting second-order terms, this matrix is no longer symmetric:

$$\widehat{K}^p = \begin{vmatrix} k_n & 0 & 0 \\ \tan\varphi_{\mathrm{g}}k_n & 0 & 0 \\ 0 & 0 & k_t \end{vmatrix} \tag{8}$$

2.4. Description of the medium's fabrics

In the proposed approach, the RVE is a statistically homogeneous medium. The location of each particle in the RVE is not known, but the direction of contacts is statistically described. In this model, the structure at the microscopic level (fabric) is completely described by the distribution functions $f_{\theta,\varphi}$ or $\omega(\theta,\varphi)$. Because of loading paths, the micro-structure of a granular assembly is likely to evolve considerably, thus modifying the macroscopic properties of the medium. Changes in fabrics occur when contacts fail, new contacts are created, or the direction of existing contacts changes. The orientation of a contact changes when the relative displacement of the centers of the two particles in contact, combining both rolling and sliding motions,

takes place. However, as a first approximation, we assume that the relative displacement of the centroids of two particles in contact contributes little to the change in the contact orientation (Jenkins and Strack, 1993). This assumption is certainly reasonable for dense media, but more debatable for loose assemblies (Bardet, 1994b; Oda et al., 1997).

Furthermore, it is now well established that a granular medium can be considered as composed of two distinct phases. Specific patterns for grains that are joined by contacts transmitting high contact forces may be developed within the granular assembly (Horne, 1965). Since these patterns are responsible for the ability of the medium to transmit local forces, they are denoted force chains (or solid paths, using the terminology adopted by Horne). These chains constitute the so-called strong phase. In the vicinity of these chains, a network of weak contacts, associated with low contact forces, exists; similarly, this network constitutes the so-called weak phase. Several authors refer to this concept, but Radjai has contributed substantially to proposing a clear physical interpretation (Radjai et al., 1998, 1999). Force chains, thus transmitting high forces, may become unstable if the surrounding weak phase does not ensure a sufficient sustaining effect. This assumption is supported by several experimental investigations (Dantu, 1957; Drescher, 1976; Oda and Konishi, 1974). As suggested by Oda et al., 1982, we can therefore conjecture that the force chains whose mean direction is close to the major principal direction of the loading may collapse when the stress level along this direction is too high. If these chains collapse, the associated contact directions can no longer hold high contact forces. As a consequence, an "extinction" cone ($-\varphi_e \leqslant \varphi \leqslant \varphi_e$), whose symmetry axis corresponds to the major principal direction of the loading, is introduced in the micro-directional model. It is assumed that no contact exists within this cone. φ_e is thereby called the extinction angle. For a more complete discussion, we refer the reader to Nicot (2003a), Nicot and Darve (2005).

Thus, the distribution function $f_{\theta,\varphi}$ will evolve, depending only on the failure that may occur in grain contacts and on the creation of new contacts. From above, the contact in direction $\vec{n}(\theta,\varphi)$ exists as long as $\widehat{F}_n(\theta,\varphi) > 0$. Furthermore, some authors (for example Dantu, 1957; Drescher, 1976; Oda and Konishi, 1974; Oda et al., 1980, 1982; Calvetti et al., 1997) have reported, as clear experimental evidence, that the production rate of new contacts in a given direction $\vec{n}(\theta,\varphi)$ within a granular assembly is proportional to the macroscopic normal strain rate in this direction:

$$\frac{\dot{\omega}(\theta,\varphi)}{\omega(\theta,\varphi)} = b\dot{\varepsilon}_{ij}n_i(\theta,\varphi)n_j(\theta,\varphi) \tag{9}$$

From a physical viewpoint, it seems reasonable to admit that the number of contacts increases along compressive directions and decreases along tensile directions, as prescribed by Eq. (9). Several authors have also pointed out that specific variables that characterize the fabric of the medium (namely, the so-called fabric tensor) could be expressed in terms of the stress tensor. As the creation of contacts is a hardening mechanism resulting from the geometrical configuration of the packing, it therefore seems relevant to express the change in the fabric in terms of kinematical variables, as other authors have done (see for instance Luding, 2004; Rothenburg and Kruyt, 2004).

Usually, Eq. (9) is also used to describe the loss of contacts in a given direction, so that Eq. (9) makes the number of contacts $\omega_e(\theta,\varphi)$ evolve, whatever the sign of $\dot{\varepsilon}_{ij}n_i(\theta,\varphi)n_j(\theta,\varphi)$. Of course, a rigorous description of the creation of new contacts requires a complete spatial description of the micro-structure in which both the location and the motion of each grain must be known. This is not possible through the proposed approach, which therefore justifies using an empirical relation such as Eq. (9). Nevertheless, the loss of contacts between grains, in a given direction, is only governed by the vanishing of $\widehat{F}_n$ between each pair of grains in contact. Consequently, a statistical description of the direction of contacts, and not of the location of grains, cannot account for the creation of new contacts, but is able to describe the loss of contacts. An relation such as Eq. (9) is thus of interest, but its range of validity can be restricted to the compressive directions: $\dot{\varepsilon}_{ij}n_i(\theta,\varphi)n_j(\theta,\varphi) > 0$.

Accordingly, it can be concluded in each direction $\vec{n}(\theta,\varphi)$:

- If $\mathrm{d}\varepsilon_{ij}n_i(\theta,\varphi)n_j(\theta,\varphi) > 0$, then $\mathrm{d}\omega_e(\theta,\varphi) = b\omega_e(\theta,\varphi)\mathrm{d}\varepsilon_{ij}n_i(\theta,\varphi)n_j(\theta,\varphi)$; new contacts are created.
- If $\mathrm{d}\varepsilon_{ij}n_i(\theta,\varphi)n_j(\theta,\varphi) \leqslant 0$ and $\widehat{F}_n(\theta,\varphi) > 0$, then $\mathrm{d}\omega_e(\theta,\varphi) = 0$; no contact fails, no contact is created.
- If $\widehat{F}_n(\theta,\varphi) \leqslant 0$, then $\omega_e(\theta,\varphi) = 0$; all contacts in direction $\vec{n}(\theta,\varphi)$ fail.

Parameter b, introduced in Eq. (9), can be determined from the definition of the number of contacts:

$$N_c = \int\int_D \omega_e(\theta,\varphi)\sin\varphi\,\mathrm{d}\varphi\,\mathrm{d}\theta \tag{10}$$

where D is the sub-domain of the domain $[0;\pi]^2$ containing the directions along which the number of contacts is not zero. After differentiation, Eq. (10) gives:

$$\mathrm{d}N_c = \int\int_D \mathrm{d}\omega_e(\theta,\varphi)\sin\varphi\,\mathrm{d}\varphi\,\mathrm{d}\theta + \int\int_{\mathrm{d}D} \omega_e(\theta,\varphi)\sin\varphi\,\mathrm{d}\varphi\,\mathrm{d}\theta \tag{11}$$

where $\mathrm{d}D$ denotes the incremental change in D during an incremental loading; thus $\mathrm{d}D$ gathers directions along which existing contacts have failed or new contacts were created. As D can be resolved in two domains, a compressive domain D_c gathering directions along which $\mathrm{d}\varepsilon_{ij}n_i(\theta,\varphi)n_j(\theta,\varphi) > 0$, and a tensile domain D_t gathering directions along which $\mathrm{d}\varepsilon_{ij}n_i(\theta,\varphi)n_j(\theta,\varphi) \leqslant 0$, Eq. (11) is expressed as:

$$\mathrm{d}N_c = \int\int_{D_c} \mathrm{d}\omega_e(\theta,\varphi)\sin\varphi\,\mathrm{d}\varphi\,\mathrm{d}\theta + \int\int_{\mathrm{d}D} \omega_e(\theta,\varphi)\sin\varphi\,\mathrm{d}\varphi\,\mathrm{d}\theta \tag{12}$$

In Eq. (12), the term $\int\int_{\mathrm{d}D}\omega_e(\theta,\varphi)\sin\varphi\,\mathrm{d}\varphi\,\mathrm{d}\theta$ depends on the sign of both quantities $\mathrm{d}\widehat{u}_n = 2r_g\mathrm{d}\varepsilon_{ij}n_i(\theta,\varphi)n_j(\theta,\varphi)$ and $\widehat{F}_n(\theta,\varphi)$. In the compressive domain D_c, $\mathrm{d}\omega_e(\theta,\varphi) = b\omega_e(\theta,\varphi)\frac{\mathrm{d}\widehat{u}_n}{2r_g}$, so that Eq. (12) yields:

$$b = 2r_g\frac{\mathrm{d}N_c - \int\int_{\mathrm{d}D}\omega_e(\theta,\varphi)\sin\varphi\,\mathrm{d}\varphi\,\mathrm{d}\theta}{\int\int_{D_c}\omega_e(\theta,\varphi)\,\mathrm{d}\widehat{u}_n(\theta,\varphi)\sin\varphi\,\mathrm{d}\varphi\,\mathrm{d}\theta} \tag{13}$$

Many studies (Field, 1963; Yanagisawa, 1983; Chang et al., 1990) have attempted to relate the mean number of contacts per grain in a cohesionless granular assembly in terms of internal variables such as compactness. Typically, such relations can be expressed in the following general form:

$$N_c = N_g g(e) \tag{14}$$

where N_c is the number of contacts in a given sample containing N_g grains; e is the void ratio of the sample. It has been shown that this type of relation may be incorrect in some cases, especially after the failure peak for dense materials. Mechanisms related to the dilatancy phenomenon occur, leading to changes in the void ratio (the volume of the material expands) without changing the contact number. However, we emphasize that our analysis concerns the pre-peak domain. As recalled in the introduction, different failure modes may occur before the plastic limit condition is reached; in this domain, experimental results tend to prove that a single relation between the void ratio and the contact number, as expressed by Eq. (14), can be regarded as a reasonable approximation.

To exemplify the general expression given in Eq. (14), the empirical relation proposed by Field, 1963 can be adopted:

$$N_c = \frac{12N_g}{1+e} \tag{15}$$

Initially, the density within the sample is equal to ρ_0; because of the change in fabric, the density is likely to change, and the current density is denoted ρ. If ρ_g is the density of grains, as $e = \frac{\rho_g}{\rho} - 1$ and $\rho = \frac{\rho_0}{1-\varepsilon_{ii}}$, Eq. (15) can also be rewritten as:

$$N_c = 12 N_g \frac{\rho_0}{\rho_g} \frac{1}{1-\varepsilon_{ii}} \tag{16}$$

From a given state of the medium's fabric, which is completely described by distribution function $f^o_{\theta,\varphi}$ or density of contacts $\omega^\circ_e(\theta,\varphi)$, as well as the initial number of contacts N^o_c existing in each RVE and the initial density ρ_0, it is thus possible to describe the changes in the medium's fabric induced by the body strains.

3. Existence of unstable directions

In this section, we investigate the constitutive structure of the model; for that, Gudehus stress response-envelopes are computed (Gudehus, 1979). Given an initial isotropic fabric, first an axisymmetric drained triaxial loading test is simulated. Then, at different loading states, strain probes in all directions with the same norm are imposed, and stress responses are computed. This procedure assesses both the elastic and plastic parts of each strain probe. The extremities of all stress-response vectors constitute a diagram, called the response-envelope. This graphical scheme characterizes the constitutive behavior at a given stress–strain state after a given loading history.

3.1. Axisymmetric analysis

3.1.1. Constitutive equations

Starting from a cylinder-like specimen (Fig. 4), the symmetric axis (x_1) is a principal axis for both the stress and strain tensors. Axes (x_2) and (x_3) are also principal axes for these tensors. As principal directions of the strain tensor remain unchanged during the test, it follows that $\mathrm{d}\widehat{u}_i = \mathrm{d}\widehat{u}_n n_i + \mathrm{d}\widehat{u}_t t_i$ and $\mathrm{d}\widehat{F}_i = \mathrm{d}\widehat{F}_n n_i + \mathrm{d}\widehat{F}_t t_i$, with:

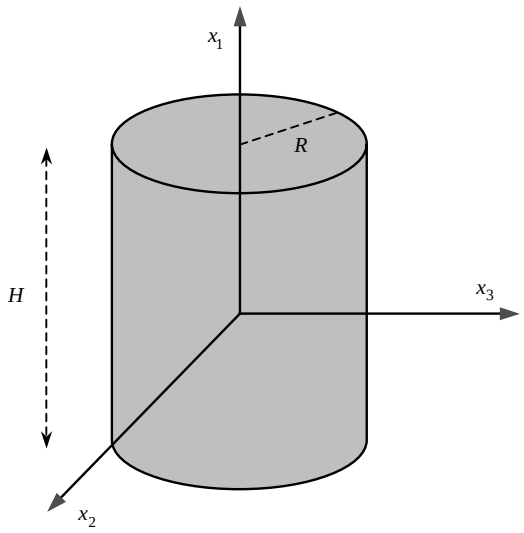

Fig. 4. Geometrical settings of the sample considered.

$$\mathrm{d}\widehat{u}_n = 2r_{\mathrm{g}}(\mathrm{d}\varepsilon_1\cos^2\varphi + \mathrm{d}\varepsilon_2\sin^2\varphi) \tag{17}$$

$$\mathrm{d}\widehat{u}_t = 2r_{\mathrm{g}}(\cos\varphi\sin\varphi(\mathrm{d}\varepsilon_1 - \mathrm{d}\varepsilon_2)) \tag{18}$$

$$\vec{t} = \begin{pmatrix} \sin\varphi \\ -\cos\varphi\cos\theta \\ -\cos\varphi\sin\theta \end{pmatrix} \tag{19}$$

Variables $\widehat{\vec{u}}$, $\widehat{\vec{\sigma}}$, and ω_e no longer depend on longitude angle θ but only on the colatitude angle φ. In these conditions, Eq. (3) gives:

$$\sigma_1 = \frac{3}{2N_{\mathrm{g}}r_{\mathrm{g}}^2}\frac{\rho_0}{\rho_{\mathrm{g}}}\frac{1}{1-\varepsilon_1-2\varepsilon_2}\int_0^{\pi}\left(\widehat{F}_n(\varphi)\cos\varphi + \widehat{F}_t(\varphi)\sin\varphi\right)\omega_e(\varphi)\cos\varphi\sin\varphi\,\mathrm{d}\varphi \tag{20}$$

$$\sigma_2 = \frac{3}{4N_{\mathrm{g}}r_{\mathrm{g}}^2}\frac{\rho_0}{\rho_{\mathrm{g}}}\frac{1}{1-\varepsilon_1-2\varepsilon_2}\int_0^{\pi}\left(\widehat{F}_n(\varphi)\sin\varphi - \widehat{F}_t(\varphi)\cos\varphi\right)\omega_e(\varphi)\sin^2\varphi\,\mathrm{d}\varphi \tag{21}$$

Differentiation of Eqs. (20), (21) yields:

$$\begin{aligned}\mathrm{d}\sigma_1 = \frac{3}{2N_{\mathrm{g}}r_{\mathrm{g}}^2}\frac{\rho_0}{\rho_{\mathrm{g}}}\int_0^{\pi}\Bigg\{&\frac{(\mathrm{d}\widehat{F}_n(\varphi)\cos\varphi + \mathrm{d}\widehat{F}_t(\varphi)\sin\varphi)\omega_e(\varphi)}{1-\varepsilon_1-2\varepsilon_2} + \frac{(\widehat{F}_n(\varphi)\cos\varphi + \widehat{F}_t(\varphi)\sin\varphi)\mathrm{d}\omega_e(\varphi)}{1-\varepsilon_1-2\varepsilon_2} \\ &+\cdots+\frac{(\widehat{F}_n(\varphi)\cos\varphi + \widehat{F}_t(\varphi)\sin\varphi)\omega_e(\varphi)(\mathrm{d}\varepsilon_1+2\mathrm{d}\varepsilon_2)}{(1-\varepsilon_1-2\varepsilon_2)^2}\Bigg\}\cos\varphi\sin\varphi\,\mathrm{d}\varphi\end{aligned} \tag{22}$$

$$\begin{aligned}\mathrm{d}\sigma_2 = \frac{3}{4N_{\mathrm{g}}r_{\mathrm{g}}^2}\frac{\rho_0}{\rho_{\mathrm{g}}}\int_0^{\pi}\Bigg\{&\frac{(\mathrm{d}\widehat{F}_n(\varphi)\sin\varphi - \mathrm{d}\widehat{F}_t(\varphi)\cos\varphi)\omega_e(\varphi)}{1-\varepsilon_1-2\varepsilon_2} + \frac{(\widehat{F}_n(\varphi)\sin\varphi - \widehat{F}_t(\varphi)\cos\varphi)\mathrm{d}\omega_e(\varphi)}{1-\varepsilon_1-2\varepsilon_2} \\ &+\cdots+\frac{(\widehat{F}_n(\varphi)\sin\varphi - \widehat{F}_t(\varphi)\cos\varphi)\omega_e(\varphi)(\mathrm{d}\varepsilon_1+2\mathrm{d}\varepsilon_2)}{(1-\varepsilon_1-2\varepsilon_2)^2}\Bigg\}\cos\varphi\sin\varphi\,\mathrm{d}\varphi\end{aligned} \tag{23}$$

with $\begin{bmatrix}\mathrm{d}\widehat{F}_n \\ \mathrm{d}\widehat{F}_t\end{bmatrix} = \begin{bmatrix}k_n & 0 \\ k_{tn} & k_{tt}\end{bmatrix}\begin{bmatrix}\mathrm{d}\widehat{u}_n \\ \mathrm{d}\widehat{u}_t\end{bmatrix}$, where $k_{tt} = k_t$, $k_{tn} = 0$ in the elastic regime, and $k_{tt} = 0$, $k_{tn} = \tan\varphi_{\mathrm{g}}k_{\mathrm{n}}$ in the plastic regime.

3.1.2. Description of the probing tests

At different values of the ratio $\eta = \frac{q}{p}$ between the deviatoric stress ($q = \sigma_1 - \sigma_2$) and the isotropic stress ($p = \frac{\sigma_1+2\sigma_2}{3}$), a strain probe test is performed (Figs. 5 and 6). α_ε (resp. α_σ) is the angle of the direction of the strain (resp. stress) increment vector with the horizontal axis (Fig. 6). For a given strain increment, in order to compute both elastic and plastic parts, the following procedure is carried out: first, starting from a state defined by $(\sqrt{2}\varepsilon_2, \varepsilon_1)$ and $(\sqrt{2}\sigma_2, \sigma_1)$, and given a strain increment $\mathrm{d}\vec{\varepsilon} = (\sqrt{2}\mathrm{d}\varepsilon_2, \mathrm{d}\varepsilon_1)$, the incremental stress response is computed using constitutive equations (22) and (23).

3.1.3. Computation of the directional second-order work

Successive axisymmetric probing tests, using data reported in Table 1, are performed at different values of $\eta = \frac{q}{p}$.

The quantity $\mathrm{d}^2W = \mathrm{d}\overline{\overline{\sigma}}\,\mathrm{d}\overline{\overline{\varepsilon}}$ is computed as a function of stress response direction α_σ. Let us note that in axisymmetric conditions, the second-order work takes the straightforward form:

$$\mathrm{d}^2W = \mathrm{d}\sigma_1\mathrm{d}\varepsilon_1 + 2\mathrm{d}\sigma_2\mathrm{d}\varepsilon_2 \tag{24}$$

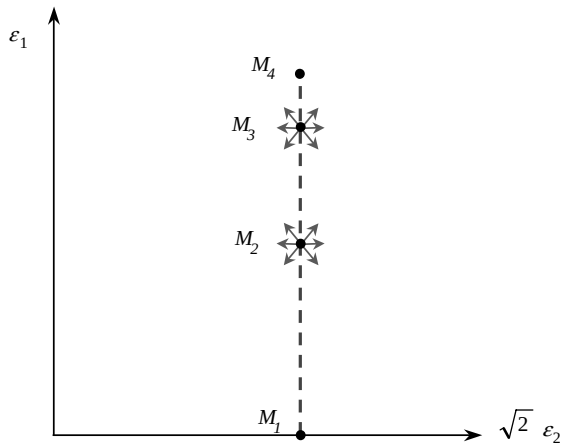

Fig. 5. Initial axisymmetric drained triaxial loading is carried out (line M_1M_4). At different states of the loading, characterized by different values of η, a strain probe test is performed (points M_2 and M_3).

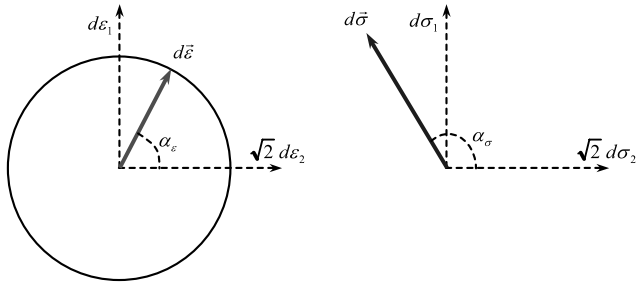

Fig. 6. Definition of Rendulic planes; strain probes and stress responses.

Table 1
Triaxial test: constitutive parameters

Initial isotropic stress (MPa)	Initial void ratio	k_n (MPa)	k_t (MPa)	φ_g (deg)
0.125	0.66	15,708	6830	15

The directional analysis aims at detecting the loading directions leading to the vanishing of the second-order work. What is the significance of this direction? It means that if the granular assembly, in a given strain–stress state after a given strain–stress history, is loaded in this direction, then a material instability in the sense of Hill (1958) may occur. In this direction, the deformation can be pursued in an infinitesimal manner (all loading conditions remaining identical) without any input of energy from external agencies. The loading mode also becomes uncontrollable in Nova's sense (Nova, 1994). The medium is thus potentially unstable, since Hill's condition of instability is only a necessary condition (not a sufficient condition), and the occurrence of instability requires that proper loading control variables be considered (i.e. specific dead loads).

As suggested by Darve and Roguiez (1998), it is useful to consider the dimensionless variable d^2w (the so-called "normalized second order work") defined as:

$$\mathrm{d}^2 w = \frac{\mathrm{d}^2 W}{\sqrt{\mathrm{d}\sigma_1^2 + 2\mathrm{d}\sigma_2^2}\sqrt{\mathrm{d}\varepsilon_1^2 + 2\mathrm{d}\varepsilon_2^2}} \tag{25}$$

which can also be understood as the cosine of the angle between the two vectors $(\sqrt{2}\mathrm{d}\varepsilon_2, \mathrm{d}\varepsilon_1)$ and $(\sqrt{2}\mathrm{d}\sigma_2, \mathrm{d}\sigma_1)$. Thus $|\mathrm{d}^2 w|$ varies between 0 and +1. The change in $\mathrm{d}^2 w$ in terms of α_σ is reported in Fig. 7. From a critical value $\eta_c \approx 0.715$, a cone in which $\mathrm{d}^2 w$ is negative exists; moreover, directions α_σ, for which $\mathrm{d}^2 w$ is negative, are similar to those observed using phenomenological constitutive models (in particular the incrementally nonlinear model or the incremental eightfold linear model; Darve and Roguiez, 1998) and following the same numerical program (Fig. 8).

3.2. Three-dimensional analysis

3.2.1. Constitutive equations

Starting from Eq. (3), a generalization of the incremental equations (22), (23) can be deduced in fully three-dimensional conditions. Combining Eqs. (3) and (16) yields:

$$\sigma_{ij} = \frac{3}{2\pi N_\mathrm{g} r_\mathrm{g}^2}\frac{\rho_0}{\rho_\mathrm{g}}\int\int_{[o;\pi]^2}\frac{\widehat{F}_i(\theta,\varphi)n_j(\theta,\varphi)\omega_e(\theta,\varphi)}{1-\varepsilon_{kk}}\sin\varphi\,\mathrm{d}\theta\,\mathrm{d}\varphi \tag{26}$$

Differentiation of Eq. (26) gives:

$$\mathrm{d}\sigma_{ij} = \frac{3}{2\pi N_\mathrm{g} r_\mathrm{g}^2}\frac{\rho_0}{\rho_\mathrm{g}}\int\int_{[o;\pi]^2}\left\{\frac{\mathrm{d}\widehat{F}_i(\theta,\varphi)n_j(\theta,\varphi)\omega_e(\theta,\varphi)}{1-\varepsilon_{kk}} + \frac{\widehat{F}_i(\theta,\varphi)n_j(\theta,\varphi)\mathrm{d}\omega_e(\theta,\varphi)}{1-\varepsilon_{kk}} + \cdots + \frac{\widehat{F}_i(\theta,\varphi)n_j(\theta,\varphi)\omega_e(\theta,\varphi)\mathrm{d}\varepsilon_{kk}}{(1-\varepsilon_{kk})^2}\right\}\sin\varphi\,\mathrm{d}\theta\,\mathrm{d}\varphi \tag{27}$$

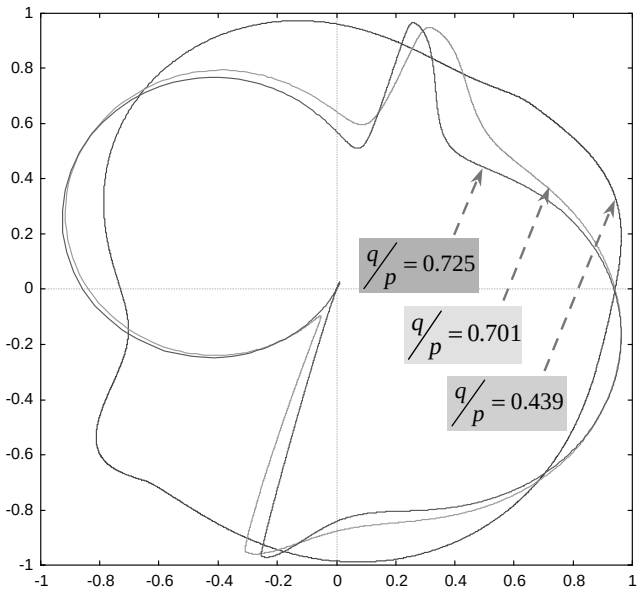

Fig. 7. Change in dimensionless second-order work in terms of α_σ; polar representation.

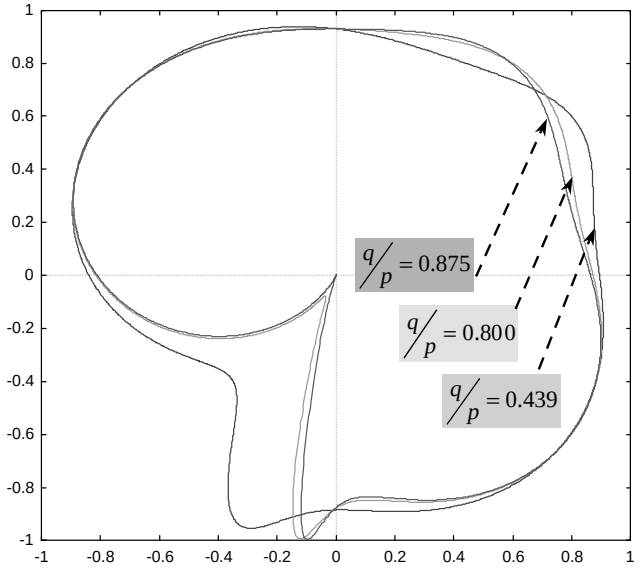

Fig. 8. Change in dimensionless second-order work in terms of α_σ; polar representation, using an incrementally nonlinear model (Darve and Roguiez, 1998).

Then it follows that:

$$\mathrm{d}\sigma_1 = \frac{3}{2\pi N_g r_g^2}\frac{\rho_0}{\rho_g}\int\int_{[0;\pi]^2}\left\{\frac{(\mathrm{d}\widehat{F}_n(\varphi)\cos\varphi + \mathrm{d}\widehat{F}_t(\varphi)\sin\varphi)\omega_e(\varphi)}{1-\varepsilon_1-\varepsilon_2-\varepsilon_3} + \cdots + \frac{(\widehat{F}_n(\varphi)\cos\varphi + \widehat{F}_t(\varphi)\sin\varphi)\mathrm{d}\omega_e(\varphi)}{1-\varepsilon_1-\varepsilon_2-\varepsilon_3}\right.$$
$$\left. + \cdots + \frac{(\widehat{F}_n(\varphi)\cos\varphi + \widehat{F}_t(\varphi)\sin\varphi)\omega_e(\varphi)(\mathrm{d}\varepsilon_1+\mathrm{d}\varepsilon_2+\mathrm{d}\varepsilon_3)}{(1-\varepsilon_1-\varepsilon_2-\varepsilon_3)^2}\right\}\cos\varphi\sin\varphi\,\mathrm{d}\varphi\,\mathrm{d}\theta \tag{28}$$

$$\mathrm{d}\sigma_2 = \frac{3}{2\pi N_g r_g^2}\frac{\rho_0}{\rho_g}\int\int_{[0;\pi]^2}\left\{\frac{(\mathrm{d}\widehat{F}_n(\varphi)\sin\varphi - \mathrm{d}\widehat{F}_t(\varphi)\cos\varphi)\omega_e(\varphi)}{1-\varepsilon_1-\varepsilon_2-\varepsilon_3} + \cdots + \frac{(\mathrm{d}\widehat{F}_n(\varphi)\sin\varphi - \mathrm{d}\widehat{F}_t(\varphi)\cos\varphi)\mathrm{d}\omega_e(\varphi)}{1-\varepsilon_1-\varepsilon_2-\varepsilon_3}\right.$$
$$\left. + \cdots + \frac{(\mathrm{d}\widehat{F}_n(\varphi)\sin\varphi - \mathrm{d}\widehat{F}_t(\varphi)\cos\varphi)\omega_e(\varphi)(\mathrm{d}\varepsilon_1+\mathrm{d}\varepsilon_2+\mathrm{d}\varepsilon_3)}{(1-\varepsilon_1-\varepsilon_2-\varepsilon_3)^2}\right\}\sin^2\varphi\cos^2\theta\,\mathrm{d}\varphi\,\mathrm{d}\theta \tag{29}$$

$$\mathrm{d}\sigma_3 = \frac{3}{2\pi N_g r_g^2}\frac{\rho_0}{\rho_g}\int\int_{[0;\pi]^2}\left\{\frac{(\mathrm{d}\widehat{F}_n(\varphi)\sin\varphi - \mathrm{d}\widehat{F}_t(\varphi)\cos\varphi)\omega_e(\varphi)}{1-\varepsilon_1-\varepsilon_2-\varepsilon_3} + \cdots + \frac{(\mathrm{d}\widehat{F}_n(\varphi)\sin\varphi - \mathrm{d}\widehat{F}_t(\varphi)\cos\varphi)\mathrm{d}\omega_e(\varphi)}{1-\varepsilon_1-\varepsilon_2-\varepsilon_3}\right.$$
$$\left. + \cdots + \frac{(\mathrm{d}\widehat{F}_n(\varphi)\sin\varphi - \mathrm{d}\widehat{F}_t(\varphi)\cos\varphi)\omega_e(\varphi)(\mathrm{d}\varepsilon_1+\mathrm{d}\varepsilon_2+\mathrm{d}\varepsilon_3)}{(1-\varepsilon_1-\varepsilon_2-\varepsilon_3)^2}\right\}\sin^2\varphi\sin^2\theta\,\mathrm{d}\varphi\,\mathrm{d}\theta \tag{30}$$

3.2.2. Description of the probing tests

Starting from a given stress–strain state obtained after the previous axisymmetric triaxial loading ($\eta = 0.706$), a fully three-dimensional probing test is performed. As previously, strain probes are imposed, and stress responses are computed. As depicted in Fig. 9, it is useful to introduce Euler's angles α_ε (resp. α_σ)

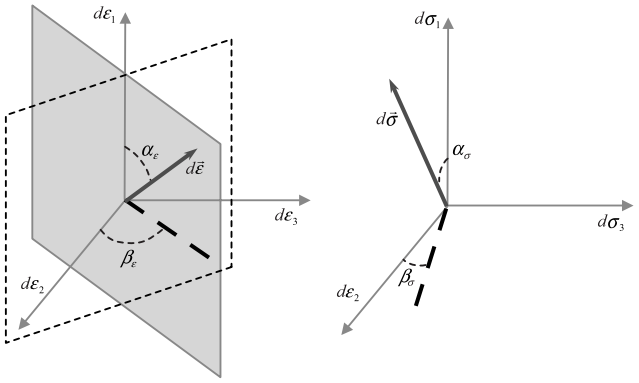

Fig. 9. Three-dimensional probing tests: strain probes and stress responses.

and β_ε (resp. β_σ), so that $\mathrm{d}\vec{\varepsilon} = \begin{bmatrix} \mathrm{d}\varepsilon_1 \\ \mathrm{d}\varepsilon_2 \\ \mathrm{d}\varepsilon_3 \end{bmatrix} = \begin{bmatrix} \mathrm{d}e\cos\alpha_\varepsilon \\ \mathrm{d}e\sin\alpha_\varepsilon\cos\beta_\varepsilon \\ \mathrm{d}e\sin\alpha_\varepsilon\sin\beta_\varepsilon \end{bmatrix}$ and $\mathrm{d}\vec{\sigma} = \begin{bmatrix} \mathrm{d}\sigma_1 \\ \mathrm{d}\sigma_2 \\ \mathrm{d}\sigma_3 \end{bmatrix} = \begin{bmatrix} \mathrm{d}s\cos\alpha_\sigma \\ \mathrm{d}s\sin\alpha_\sigma\cos\beta_\sigma \\ \mathrm{d}s\sin\alpha_\sigma\sin\beta_\sigma \end{bmatrix}$. Note that in axisymmetric conditions, $\beta_\varepsilon = \beta_\sigma = \frac{\pi}{4}$.

Stress responses were analyzed with $\mathrm{d}\vec{\varepsilon}$ belonging to N successive planes (P_i^ε) defined by the equation $\beta_\varepsilon = \frac{\pi}{4} + i\Delta\beta = \frac{\pi}{4} + i\frac{\pi}{N}$, $i \in \{0, \ldots, N-1\}$. In each plane (P_i^ε), α_ε varies in the range of $[0; 2\pi]$. The simulations presented in this paper were carried out with $N = 20$. The resulting stress $\mathrm{d}\vec{\sigma}$ is computed as a response to each of these particular two-dimensional strain probing tests.

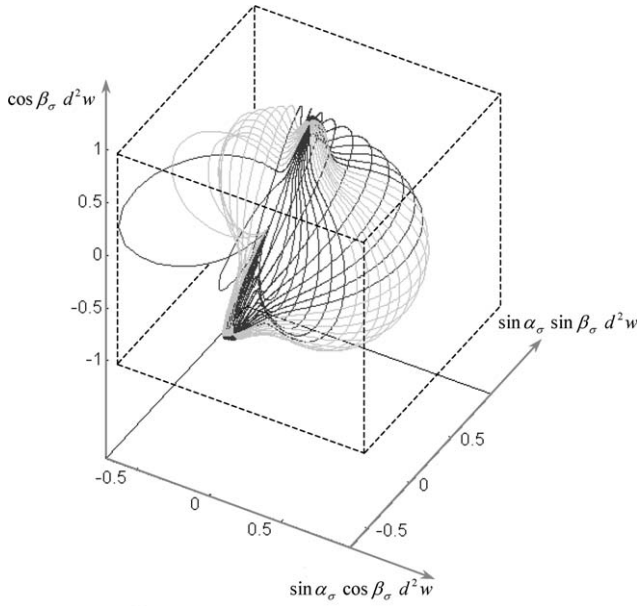

Fig. 10. Variations of normalized second-order work in terms of both angles α_σ and β_σ; polar representation.

3.2.3. Existence of a thin unstable cone

Starting from an axisymmetric state defined by $\eta = 0.725$, the sign of second-order work is now analyzed when the strain probe belongs to different planes (P_i^{ε}), with $N = 20$. We denote (W_i) the curve joining in the physical frame (x_2, x_3, x_1) the points $(\sin\alpha_\sigma \cos\beta_\sigma \mathrm{d}^2 w, \sin\alpha_\sigma \sin\beta_\sigma \mathrm{d}^2 w, \cos\alpha_\sigma \mathrm{d}^2 w)$ when the strain probe $\mathrm{d}\vec{\varepsilon}$

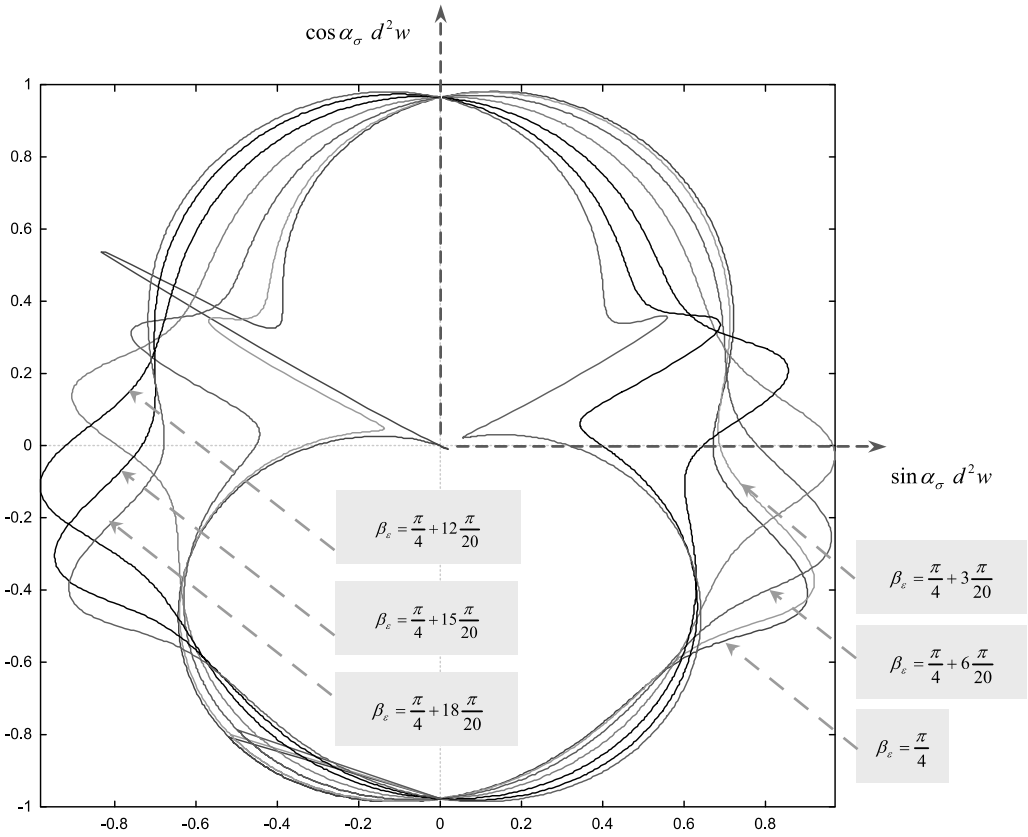

Fig. 11. Normalized second-order work in terms of α_σ; polar representation.

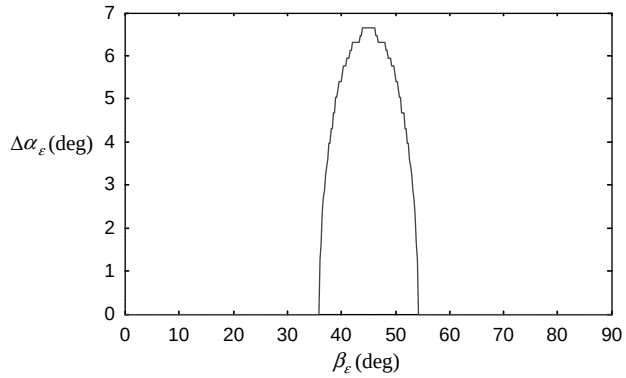

Fig. 12. Variations in the angular width $\Delta\alpha_\varepsilon$ of the sector in which $\mathrm{d}^2 W < 0$ in terms of β_ε.

belongs to the plane (P_i^e). The general shape of these curves is depicted in Fig. 10. For the sake of expediency, plane curves ($\sin\alpha_\sigma\, \mathrm{d}^2w$, $\cos\alpha_\sigma\, \mathrm{d}^2w$) were plotted in Fig. 11, which shows that the second-order work always remains positive if the strain probe belongs to a plane (P_i^e) whose orientation β_ε is not close to the orientation of the bisector plane (i.e., the Rendulic plane). It can thereby be conjectured that the strain probe directions along which the second-order work is negative are contained in a slightly expanded cone with respect to the bisector plane (corresponding to $\beta_\varepsilon = \frac{\pi}{4}$). This result is confirmed in Fig. 12, where the variations of $\Delta\alpha_\varepsilon$, corresponding to the angular width of the sector of the plane (P_i^e) in which $\mathrm{d}^2W < 0$, are given in terms of β_ε. This symmetric sine-like curve is maximal for $\beta_\varepsilon = \frac{\pi}{4}$ and rapidly tends toward 0 when $\beta_\varepsilon \neq \frac{\pi}{4}$. Typically, $\Delta\alpha_\varepsilon$ is different from the zero value over the range $[36°; 54°]$. This means that after a given axisymmetric loading, material instability can occur only along loading increments that nearly respect axisymmetric conditions.

4. Micro-mechanical interpretation

4.1. Micro- and macro-level second-order works

Hill's material instability criterion, even if it is not established on a thermodynamical basis, has been widely discussed and used (Nova, 1994; Darve and Laouafa, 2000; Darve et al., 2004). This criterion can be considered as a generalization of the postulate introduced by Drucker (Drucker, 1951). Mandel attempted to apply Drucker's postulate to granular materials and showed that this postulate was violated if a frictional contact model was used at the interface of the granules, thus showing that Hill's material instability might occur within granular masses (Mandel, 1966). The fact that the micro-directional model is essentially built from a particle description is very advantageous, because one can search for a possible relation between the existence of couples $(\mathrm{d}\vec{\sigma}, \mathrm{d}\vec{\varepsilon})$ verifying $\mathrm{d}^2W < 0$ and micro-structural arguments.

Let us consider again Eq. (27), which can be resolved as $\mathrm{d}\sigma_{ij} = \mathrm{d}\sigma'_{ij} + \mathrm{d}\sigma''_{ij} + \mathrm{d}\sigma'''_{ij}$, with:

$$\mathrm{d}\sigma'_{ij} = \frac{3}{2\pi N_\mathrm{g} r_\mathrm{g}^2}\frac{\rho_0}{\rho_\mathrm{g}}\int\int_{[o;\pi]^2}\frac{\mathrm{d}\widehat{F}_i(\theta,\varphi)n_j(\theta,\varphi)\omega_e(\theta,\varphi)}{1-\varepsilon_{kk}}\sin\varphi\,\mathrm{d}\theta\,\mathrm{d}\varphi \tag{31}$$

$$\mathrm{d}\sigma''_{ij} = \frac{3}{2\pi N_\mathrm{g} r_\mathrm{g}^2}\frac{\rho_0}{\rho_\mathrm{g}}\int\int_{[o;\pi]^2}\frac{\widehat{F}_i(\theta,\varphi)n_j(\theta,\varphi)\omega_e(\theta,\varphi)\mathrm{d}\varepsilon_{kk}}{(1-\varepsilon_{kk})^2}\sin\varphi\,\mathrm{d}\theta\,\mathrm{d}\varphi \tag{32}$$

$$\mathrm{d}\sigma'''_{ij} = \frac{3}{2\pi N_\mathrm{g} r_\mathrm{g}^2}\frac{\rho_0}{\rho_\mathrm{g}}\int\int_{[o;\pi]^2}\frac{\widehat{F}_i(\theta,\varphi)n_j(\theta,\varphi)\mathrm{d}\omega_e(\theta,\varphi)}{1-\varepsilon_{kk}}\sin\varphi\,\mathrm{d}\theta\,\mathrm{d}\varphi \tag{33}$$

Thus, taking advantage of the kinematic localization given in Eq. (4), the second-order work can be expressed as:

$$\mathrm{d}^2W = \mathrm{d}^2W_\mathrm{l} + \mathrm{d}^2W_\mathrm{v} + \mathrm{d}^2W_\mathrm{f} \tag{34}$$

where:

$$\mathrm{d}^2W_\mathrm{l} = \frac{3}{2\pi N_\mathrm{g} r_\mathrm{g}^2}\frac{\rho_0}{\rho_\mathrm{g}}\int\int_{[o;\pi]^2}\frac{\mathrm{d}\widehat{F}_i(\theta,\varphi)\,\mathrm{d}\widehat{u}_i(\theta,\varphi)\omega_e(\theta,\varphi)}{1-\varepsilon_{kk}}\sin\varphi\,\mathrm{d}\theta\,\mathrm{d}\varphi \tag{35}$$

$$\mathrm{d}^2W_\mathrm{v} = \frac{3}{2\pi N_\mathrm{g} r_\mathrm{g}^2}\frac{\rho_0}{\rho_\mathrm{g}}\int\int_{[o;\pi]^2}\frac{\widehat{F}_i(\theta,\varphi)\,\mathrm{d}\widehat{u}_i(\theta,\varphi)\omega_e(\theta,\varphi)\mathrm{d}\varepsilon_{kk}}{(1-\varepsilon_{kk})^2}\sin\varphi\,\mathrm{d}\theta\,\mathrm{d}\varphi \tag{36}$$

$$\mathrm{d}^2W_\mathrm{f} = \frac{3}{2\pi N_\mathrm{g} r_\mathrm{g}^2}\frac{\rho_0}{\rho_\mathrm{g}}\int\int_{[o;\pi]^2}\frac{\widehat{F}_i(\theta,\varphi)\,\mathrm{d}\widehat{u}_i(\theta,\varphi)\mathrm{d}\omega_e(\theta,\varphi)}{1-\varepsilon_{kk}}\sin\varphi\,\mathrm{d}\theta\,\mathrm{d}\varphi \tag{37}$$

The term d^2W_l can be interpreted as the average of the local directional second-order work $\mathrm{d}^2\widehat{W} = \mathrm{d}\widehat{F}_i\,\mathrm{d}\widehat{u}_i$ in each contact direction. It constitutes the main part of the macroscopic second-order work. The term

d^2W_v accounts for the sample's change in volume, and the term d^2W_f is related to the change in the medium's fabric. Eqs. (34)–(37), on the one hand, relate the macroscopic second-order work to micro-structural aspects, and on the other hand show that the macroscopic second-order work cannot be considered the single average of local second-order works but also depends on the changes in both the volume and fabric of the medium. The macroscopic second-order work, which refers to the concept of material instability, is therefore influenced not only by a material cause (d^2W_l), but also by geometric sources (d^2W_v and d^2W_f).

From the analysis of Fig. 13, we can conjecture that the last term, d^2W_f, is negligible with respect to the other two, d^2W_l and d^2W_v. On the contrary, this figure reveals that the term d^2W_v cannot be neglected in Eq. (34) and contributes significantly to the global macroscopic second-order work. Moreover, the single term d^2W_l never vanishes, even if the shape of the d^2W_l curve is rather close to that of the d^2W curve. In the following, we focus on the term d^2W_l, and we show that a notable correlation can be exhibited between the directional local second-order work $d^2\widehat{W}$ (assessed for each contact direction, using directional variables) and the macroscopic part d^2W_l.

4.2. The local second-order work

In the $(\vec{n},\vec{t}_1,\vec{t}_2)$ frame, we have the decomposition $d\widehat{\vec{F}} = d\widehat{F}_n\vec{n} + d\widehat{F}_{t_1}\vec{t}_1 + d\widehat{F}_{t_2}\vec{t}_2$ and $d\widehat{\vec{u}} = d\widehat{u}_n\vec{n} + d\widehat{u}_{t_1}\vec{t}_1 + d\widehat{u}_{t_2}\vec{t}_2$, then it follows that:

$$d^2\widehat{W} = d\widehat{\vec{F}}\cdot d\widehat{\vec{u}} = d\widehat{F}_n d\widehat{u}_n + d\widehat{F}_{t_1} d\widehat{u}_{t_1} + d\widehat{F}_{t_2} d\widehat{u}_{t_2} \tag{38}$$

In the elastic case, Eq. (38) takes the trivial form

$$d^2\widehat{W} = k_n d\widehat{u}_n^2 + k_t d\widehat{u}_t^2 \tag{39}$$

which is a definite positive quadratic form where the notation $d\widehat{u}_t = \|d\widehat{\vec{u}}_t\|$ is employed. Thus, whichever contact direction is considered, $d^2\widehat{W} \geqslant 0$ in the elastic regime. On the other hand, in the plastic case, Eq. (38) reveals that $d^2\widehat{W}$ is a quadratic form that can be positive or negative, with respect to the sign of discriminant Δ:

$$d^2\widehat{W} = k_n d\widehat{u}_n^2 + \tan\varphi_g \cos\alpha k_n d\widehat{u}_n d\widehat{u}_t + k_t \sin^2\alpha d\widehat{u}_t^2 \tag{40}$$

where α is the angle between both vectors $\vec{t}_1 = \dfrac{\widehat{\vec{F}}_t}{\|\widehat{\vec{F}}_t\|}$ and $d\widehat{\vec{u}}_t$ (as defined in Fig. 3).

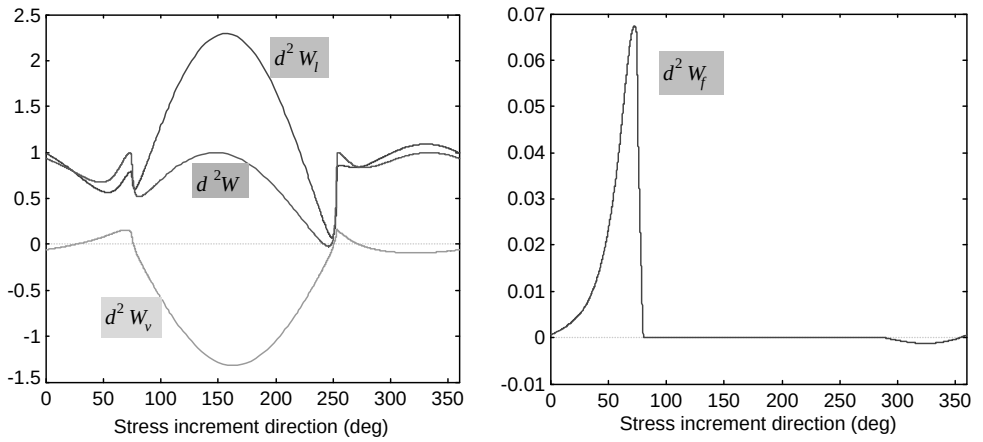

Fig. 13. Decomposition of the macroscopic second-order work.

The discriminant Δ is equal to $(\tan\varphi_g \cos\alpha k_n \mathrm{d}\widehat{u}_n)^2\left(1-4\frac{k_t\tan^2\alpha}{k_n\tan^2\varphi_g}\right)$; it is positive if $|\tan\alpha| \leqslant \frac{\tan\varphi_g}{2}\sqrt{\frac{k_n}{k_t}}$. If this condition is fulfilled, $\mathrm{d}^2\widehat{W}$ vanishes for two values of $\mathrm{d}\widehat{u}_t$:

$$U_1 = \frac{-\tan\varphi_g k_n\left(\mathrm{d}\widehat{u}_n\cos\alpha + |\mathrm{d}\widehat{u}_n\cos\alpha|\sqrt{1-4\frac{k_t\tan^2\alpha}{k_n\tan^2\varphi_g}}\right)}{2k_t\sin^2\alpha} \tag{41}$$

$$U_2 = \frac{-\tan\varphi_g k_n\left(\mathrm{d}\widehat{u}_n\cos\alpha - |\mathrm{d}\widehat{u}_n\cos\alpha|\sqrt{1-4\frac{k_t\tan^2\alpha}{k_n\tan^2\varphi_g}}\right)}{2k_t\sin^2\alpha} \tag{42}$$

If $\mathrm{d}\widehat{u}_n\cos\alpha \geqslant 0$, U_1 and U_2 are negative, which implies that $\forall\,\mathrm{d}\widehat{u}_t \geqslant 0$, $\mathrm{d}^2\widehat{W} \geqslant 0$. Let us now consider the other case, $\mathrm{d}\widehat{u}_n\cos\alpha < 0$; U_1 and U_2 are positive, which implies that $\forall\,\mathrm{d}\widehat{u}_t \in [U_1;U_2]$, $\mathrm{d}^2\widehat{W} \leqslant 0$.

Moreover, the local plastic condition is written $\|\widehat{\vec{F}}_t + k_k\,\mathrm{d}\widehat{\vec{u}}_t\| \geqslant \tan\varphi_g(\widehat{F}_n + k_n\,\mathrm{d}\widehat{u}_n)$, which, ignoring second-order terms (see Appendix B), yields:

$$\mathrm{d}\widehat{u}_n \leqslant \frac{k_t\,\mathrm{d}\widehat{u}_t}{k_n\tan\varphi_g}\cos\alpha \tag{43}$$

If $\cos\alpha < 0$, then $\mathrm{d}\widehat{u}_n < 0$, which implies that $\mathrm{d}\widehat{u}_n\cos\alpha \geqslant 0$, and accordingly $\forall\,\mathrm{d}\widehat{u}_t \geqslant 0$, $\mathrm{d}^2\widehat{W} \geqslant 0$. As a consequence, condition $\mathrm{d}^2\widehat{W} < 0$ requires that $\cos\alpha \geqslant 0$ and $\mathrm{d}\widehat{u}_n \leqslant 0$.

In conclusion, the local second-order work is negative if the three following conditions are fulfilled at the same time:

(a) $\mathrm{d}\widehat{u}_n \leqslant 0$.

(b) $\tan\alpha \leqslant \frac{\tan\varphi_g}{2}\sqrt{\frac{k_n}{k_t}}$ with $\alpha \in \left[-\frac{\pi}{2};\frac{\pi}{2}\right]$.

(c) $\mathrm{d}\widehat{u}_t \in [U_1;U_2]$ with $U_i = \dfrac{-\tan\varphi_g k_n\,\mathrm{d}\widehat{u}_n\cos\alpha\left(1+\xi_i\sqrt{1-4\frac{k_t\tan^2\alpha}{k_n\tan^2\varphi_g}}\right)}{2k_t\sin^2\alpha}$ $(\xi_1=-1,\ \xi_2=1)$.

It can be noted that U_1 increases with α, and U_2 decreases with α (Fig. 14). Moreover, when $\alpha = 0$, $U_1 = \frac{-\mathrm{d}\widehat{u}_n}{\tan\varphi_g}$ and $U_2 \to \infty$, and when $\alpha = \arctan\left(\frac{\tan\varphi_g}{2}\sqrt{\frac{k_n}{k_t}}\right)$, $U_1 = U_2 = \frac{-2\,\mathrm{d}\widehat{u}_n\sqrt{1+\frac{\tan^2\varphi_g}{4}\frac{k_n}{k_t}}}{\tan\varphi_g}$. To ensure $\mathrm{d}^2\widehat{W} < 0$, $\mathrm{d}\widehat{u}_t$ must belong to a range whose amplitude decreases when α varies from 0 to the limit value $\arctan\left(\frac{\tan\varphi_g}{2}\sqrt{\frac{k_n}{k_t}}\right)$.

As a conclusion, when α increases, the conditions necessary to obtain $\mathrm{d}^2\widehat{W} < 0$ become more restrictive. Over an axisymmetric probing test, $\alpha = 0$, and for some values of α_σ, it is not surprising to observe that $\mathrm{d}^2\widehat{W} < 0$ (see a more complete discussion in the next section). Over a fully three-dimensional probing test, it can be shown (see Appendix C) that:

$$\tan\alpha = \frac{\sin 2\theta\sin\alpha_\varepsilon\sin\left(\beta_\varepsilon-\frac{\pi}{4}\right)}{\cos\varphi\left(\sqrt{2}\cos\alpha_\varepsilon + \sin\alpha_\varepsilon\cos\left(\beta_\varepsilon-\frac{\pi}{4}\right) + \cos 2\theta\sin\alpha_\varepsilon\sin\left(\beta_\varepsilon-\frac{\pi}{4}\right)\right)} \tag{44}$$

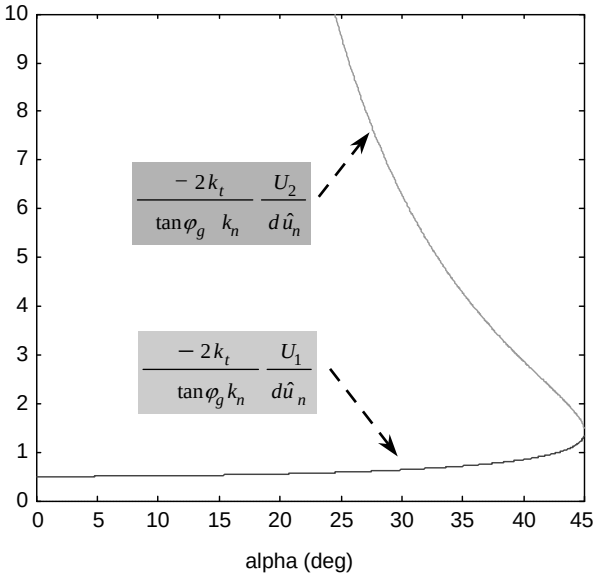

Fig. 14. U_1 and U_2 versus α; the simulation used $\frac{4k_t}{\tan^2\varphi_g k_n} = 1$.

Obviously, the amplitude of α is likely to differ from 0 when $\beta_\varepsilon \neq \frac{\pi}{4}$ and when angles θ, φ, and α_ε vary within their definition ranges. As a consequence, recalling that the term d^2W_1 has a preponderant influence on the macroscopic second-order work, the same conclusions hold true as well for d^2W, confirming the numerical evidence that the domain in which $\mathrm{d}^2W < 0$ is slightly expanded with respect to the bisector plane $\beta_\varepsilon = \frac{\pi}{4}$.

4.3. Some further comments in axisymmetric conditions

In axisymmetric conditions, it was established that $\mathrm{d}^2\widehat{W} < 0$ if the inequality $\mathrm{d}\widehat{u}_t \geqslant \dfrac{-\mathrm{d}\widehat{u}_n}{\tan\varphi_\mathrm{g}}$ is fulfilled (Section 4.2). Taking advantage of Eqs. (17) and (18), this inequality can be expressed as:

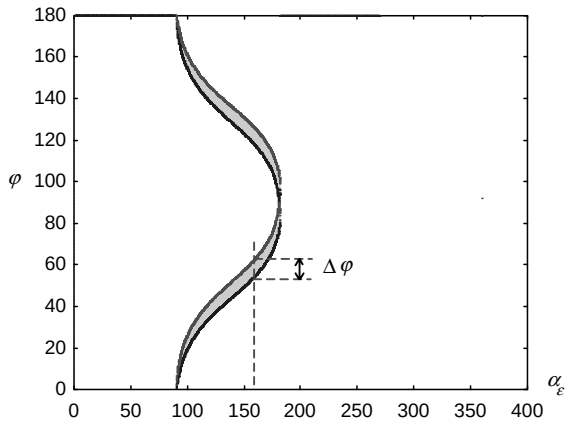

Fig. 15. Representation of the domain $D_{(\alpha_\varepsilon,\varphi)}$, computed using $\varphi_\mathrm{g} = 15°$.

$$\cos\varphi\sin\varphi\left(\cos\alpha_\varepsilon-\frac{\sqrt{2}}{2}\sin\alpha_\varepsilon\right)\geqslant-\frac{\cos^2\varphi\cos\alpha_\varepsilon+\frac{\sqrt{2}}{2}\sin^2\varphi\sin\alpha_\varepsilon}{\tan\varphi_g}\geqslant 0 \tag{45}$$

The domain $D_{(\alpha_\varepsilon,\varphi)}$ in which inequality (45) is satisfied is depicted in Fig. 15; this domain, wrapped by two curves, contains all points $(\alpha_\varepsilon,\varphi)$ satisfying inequality (45). It appears that contact directions along which $d^2\widehat{W}<0$ exist only if $\alpha_\varepsilon\in\left[\frac{\pi}{2};\pi\right]$. Let us now consider the macroscopic scale and again the axisymmetric probing test performed from $\eta=0.725$. The polar representation of the second-order work is given in Fig. 7. This diagram can also be plotted by considering the strain probe direction α_ε. We observe that the macroscopic second-order work is negative within a cone also belonging to the range $\left[\frac{\pi}{2};\pi\right]$, namely for α_ε ranges in [135–150°] (Fig. 16). This result confirms, at least in axisymmetric conditions, that the mac-

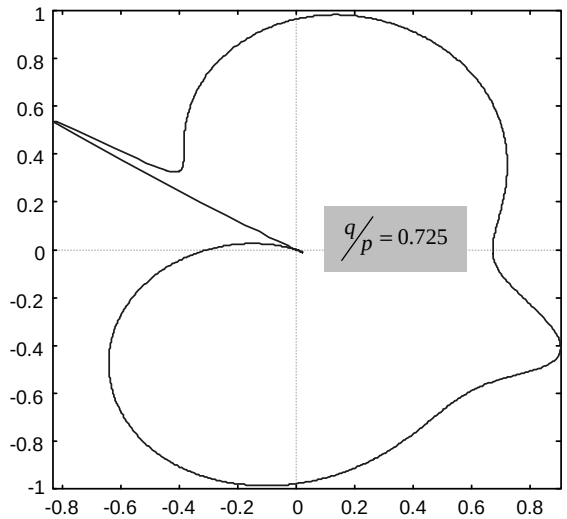

Fig. 16. d^2W in terms of α_ε; polar representation.

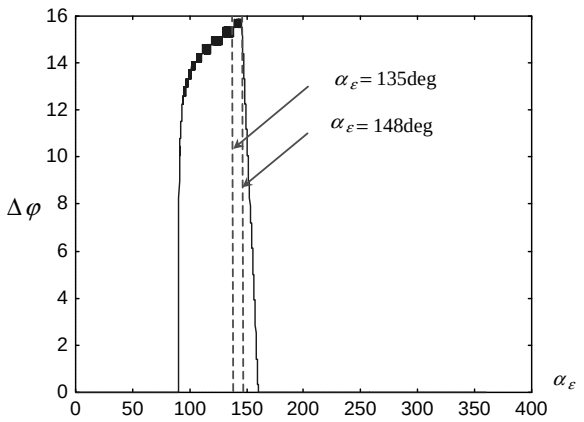

Fig. 17. Amplitude of the domain $D_{(\alpha_\varepsilon,\varphi)}$ in terms of α_ε.

roscopic second-order work is strongly influenced by the local one. Moreover, the domain $D_{(\alpha_\varepsilon,\varphi)}$ depicted in Fig. 15 was computed by considering the entire range $[0;\pi]$ for angle φ. But as already suggested, some contact directions fail in both tensile and compressive domains, reducing this range to the domain $[\varphi_e;\varphi_t]\cup[\pi-\varphi_e;\pi-\varphi_t]$. If this novel restriction is accounted for, it can be shown (Fig. 17) that the amplitude $\Delta\varphi$ of the domain $D_{(\alpha_\varepsilon,\varphi)}$ is maximum for α_ε ranges in [135–148°.], which is very close to the range corresponding to $d^2W<0$, namely [135–150°].

5. Concluding remarks

This paper has attempted to investigate the notion of material instability, developed by Hill, using a multi-scale model, the so-called micro-directional model. It was shown that, after an axisymmetric drained triaxial loading, unstable directions could exist within a cone, slightly extended around the bisector plane. A remarkable analogy was obtained, in axisymmetric conditions, with the results provided from phenomenological models such as incrementally nonlinear models. The structure of the micro-directional model has allowed a micro-mechanical interpretation to be given. Decomposing the macroscopic second-order work has highlighted that, as far as granular materials are concerned, the macroscopic second-order work could not be understood as the single summation of all the local second-order works on each contact direction; other terms account for the change in volume and fabric. Furthermore, the essential influence of the local second-order work was brought out, thereby developing a micromechanical understanding for the notion of material instability.

Basically, the micro-directional model considers that each contact between adjoining particles can be regarded as the fundamental constitutive unit of the grain assembly. The macroscopic behavior is obtained by integrating each contact (or contact direction) using a homogenization procedure, accounting for the fabric and its evolution during a loading history. The rolling motion of particles was omitted in our approach. It is well-known that the rolling of particles is responsible to a large extent for the so-called buckling effect (Oda et al., 1982, and more recently, Tordesillas and Walsh, 2002). This is supported by strong experimental evidence, together with numerical results obtained from discrete analyses. Nevertheless, we emphasize that in this paper we investigate the occurrence of the vanishing of the second-order work before the plastic limit condition is reached. As clearly pointed out by Bardet (Bardet, 1994), the rotation of particles does not play a very significant role before the localization condition is reached. Hence, the main mechanism responsible for the vanishing of the second-order work seems to be the local Coulomb friction condition.

Finally, the micro-directional model, whose constitutive ingredients are entirely concentrated on the level of particle contact, is able to reveal how the salient aspects of granular media, often requiring highly complicated developments within phenomenological approaches, are related to the behavior of the elementary constitutive unit, namely the contact behavior. The micro-directional model could give rise to a better understanding (i.e., based on elementary physics), in the mechanics of granular materials, of classic concepts such as incremental non-linearity, yield surface, flow rule, hardening mechanisms, and material instability. This last point was illustrated in this paper.

Acknowledgements

The authors are grateful to the French Ministries of Research and Civil Engineering (RGCU) for the support provided through the national research project PIR (Rock Instabilities Prevention). The French Federative Research Structure RNVO (Natural Hazards and Structure Vulnerability) is also gratefully acknowledged by the authors.

Appendix A

Eq. (5b) is the subject of analysis. Let us distinguish two cases:

- The elastic case
  Eq. (5b) gives $\mathrm{d}\widehat{F}_t = k_t \mathrm{d}\widehat{\vec{u}}_t$, which yields Eq. (7), namely $\widehat{K}^e = \begin{vmatrix} k_n & 0 & 0 \\ 0 & k_t & 0 \\ 0 & 0 & k_t \end{vmatrix}$.
- The plastic case
  Eq. (5b) gives $\mathrm{d}\widehat{\vec{F}}_t = \tan\varphi_g(F_n + k_n \mathrm{d}u_n)\dfrac{\widehat{\vec{F}}_t + k_t \mathrm{d}\widehat{\vec{u}}_t}{\|\widehat{\vec{F}}_t + k_t \mathrm{d}\widehat{\vec{u}}_t\|} - \widehat{\vec{F}}_t$, and by rearranging the terms it can be rewritten as:

$$\mathrm{d}\widehat{\vec{F}}_t = \left(\frac{\tan\varphi_g(\widehat{F}_n + k_n \mathrm{d}\widehat{u}_n)}{\|\widehat{\vec{F}}_t + k_t \mathrm{d}\widehat{\vec{u}}_t\|} - 1\right)\widehat{\vec{F}}_t + \frac{\tan\varphi_g(\widehat{F}_n + k_n \mathrm{d}\widehat{u}_n)}{\|\widehat{\vec{F}}_t + k_t \mathrm{d}\widehat{\vec{u}}_t\|} k_t \mathrm{d}\widehat{\vec{u}}_t \tag{A.1}$$

By ignoring second-order terms,

$$\left\|\widehat{\vec{F}}_t + k_t \mathrm{d}\widehat{\vec{u}}_t\right\| \approx \left\|\widehat{\vec{F}}_t\right\|\left(1 + \cos\alpha k_t \left\|\frac{\mathrm{d}\widehat{\vec{u}}_t}{\widehat{\vec{F}}_t}\right\|\right) \tag{A.2}$$

which, combining with Eq. (A.1), gives:

$$\begin{aligned}\mathrm{d}\widehat{\vec{F}}_t = {} & \left(\frac{\tan\varphi_g(\widehat{F}_n + k_n \mathrm{d}\widehat{u}_n)}{\left\|\widehat{\vec{F}}_t\right\|}\left(1 - \cos\alpha k_t \left\|\frac{\mathrm{d}\widehat{\vec{u}}_t}{\widehat{\vec{F}}_t}\right\|\right) - 1\right)\widehat{\vec{F}}_t + \cdots \\ & + \tan\varphi_g(\widehat{F}_n + k_n \mathrm{d}\widehat{u}_n)\left(1 - \cos\alpha k_t \left\|\frac{\mathrm{d}\widehat{\vec{u}}_t}{\widehat{\vec{F}}_t}\right\|\right)\frac{k_t \mathrm{d}\widehat{\vec{u}}_t}{\left\|\widehat{\vec{F}}_t\right\|} + \cdots\end{aligned} \tag{A.3}$$

and finally:

$$\mathrm{d}\widehat{\vec{F}}_t = \left(\frac{\tan\varphi_g \widehat{F}_n - \left\|\widehat{\vec{F}}_t\right\|}{\left\|\widehat{\vec{F}}_t\right\|} + \frac{\tan\varphi_g k_n \mathrm{d}\widehat{u}_n}{\left\|\widehat{\vec{F}}_t\right\|} - \cos\alpha \frac{\tan\varphi_g \widehat{F}_n k_t \left\|\mathrm{d}\widehat{\vec{u}}_t\right\|}{\left\|\widehat{\vec{F}}_t\right\|^2}\right)\widehat{\vec{F}}_t + \frac{\tan\varphi_g k_t}{\left\|\widehat{\vec{F}}_t\right\|}\mathrm{d}\widehat{\vec{u}}_t \tag{A.4}$$

But noting that $\mathrm{d}\widehat{\vec{u}}_t = \mathrm{d}\widehat{u}_{t_1}\vec{t}_1 + \mathrm{d}\widehat{u}_{t_2}\vec{t}_2 = \left\|\mathrm{d}\widehat{\vec{u}}_t\right\|\left(\cos\alpha\vec{t}_1 + \sin\alpha\vec{t}_2\right)$, Eq. (A.4) can be transformed into:

$$\mathrm{d}\widehat{\vec{F}}_t = \left(\tan\varphi_g \widehat{F}_n - \left\|\widehat{\vec{F}}_t\right\| + \tan\varphi_g k_n \mathrm{d}\widehat{u}_n\right)\vec{t}_1 + \frac{\tan\varphi_g \widehat{F}_n}{\left\|\widehat{\vec{F}}_t\right\|} k_t \mathrm{d}\widehat{u}_{t_2}\vec{t}_2 \tag{A.5}$$

which implies that:

$$\widehat{K}^p = \begin{bmatrix} k_n & 0 & 0 \\ \tan\varphi_g k_n & \dfrac{\tan\varphi_g \widehat{F}_n - \left\|\widehat{\vec{F}}_t\right\|}{\mathrm{d}\widehat{u}_{t_1}} & 0 \\ 0 & 0 & \dfrac{\tan\varphi_g \widehat{F}_n}{\left\|\widehat{\vec{F}}_t\right\|} k_t \end{bmatrix} \tag{A.6}$$

As $\|\widehat{\vec{F}}_t\| = \tan\varphi_g \widehat{F}_n$, then $\widehat{K}^p = \begin{bmatrix} k_n & 0 & 0 \\ \tan\varphi_g k_n & 0 & 0 \\ 0 & 0 & k_t \end{bmatrix}$.

Appendix B

Les us consider inequality $\|\widehat{\vec{F}}_t + k_k \mathrm{d}\widehat{\vec{u}}_t\| \geqslant \tan\varphi_g(\widehat{F}_n + k_n \mathrm{d}\widehat{u}_n)$. By squaring the two members, it follows that, as $\widehat{\vec{F}}_t = \left\|\widehat{\vec{F}}_t\right\|\vec{t}_1$:

$$\left\|\widehat{\vec{F}}_t\right\|^2 + 2\left\|\widehat{\vec{F}}_t\right\|k_k\left\|\mathrm{d}\widehat{\vec{u}}_t\right\|\cos\alpha + \left(k_k\left\|\mathrm{d}\widehat{\vec{u}}_t\right\|\right)^2 \geqslant \tan^2\varphi_g\left(\widehat{F}_n^2 + 2\widehat{F}_n k_n \mathrm{d}\widehat{u}_n + k_n^2 \mathrm{d}\widehat{u}_n^2\right) \tag{B.1}$$

Assume again that $\|\widehat{\vec{F}}_t\| = \tan\varphi_g \widehat{F}_n$, in ignoring second-order terms, yields:

$$k_t\left\|\mathrm{d}\widehat{\vec{u}}_t\right\|\cos\alpha \geqslant \tan\varphi_g k_n \mathrm{d}\widehat{u}_n \tag{B.2}$$

which allows inequality (43) to be established.

Appendix C

Les us consider an incremental strain $\mathrm{d}\vec{\vec{\varepsilon}} = \begin{bmatrix} \mathrm{d}\varepsilon_1 & 0 & 0 \\ 0 & \mathrm{d}\varepsilon_2 & 0 \\ 0 & 0 & \mathrm{d}\varepsilon_3 \end{bmatrix}$. In fully three-dimensional conditions, the definition of $\mathrm{d}\widehat{\vec{u}}_t$ is written:

$$\frac{\mathrm{d}\widehat{\vec{u}}_t}{2r_g} = \mathrm{d}\vec{\vec{\varepsilon}}\circ\vec{n} - \left(\mathrm{d}\vec{\vec{\varepsilon}}\circ\vec{n}\right)\cdot\vec{n}\vec{n} = \begin{bmatrix} \cos\varphi\sin^2\varphi(\mathrm{d}\varepsilon_1 - \cos^2\theta\,\mathrm{d}\varepsilon_2 - \sin^2\theta\,\mathrm{d}\varepsilon_3) \\ \cos\theta\sin\varphi(\mathrm{d}\varepsilon_2 - \cos^2\varphi\,\mathrm{d}\varepsilon_1 - \sin^2\varphi(\cos^2\theta\,\mathrm{d}\varepsilon_2 + \sin^2\theta\,\mathrm{d}\varepsilon_3)) \\ \sin\theta\sin\varphi(\mathrm{d}\varepsilon_3 - \cos^2\varphi\,\mathrm{d}\varepsilon_1 - \sin^2\varphi(\cos^2\theta\,\mathrm{d}\varepsilon_2 + \sin^2\theta\,\mathrm{d}\varepsilon_3)) \end{bmatrix}$$

which can be expressed as:

$$\frac{\mathrm{d}\widehat{\vec{u}}_t}{2r_g} = \cos\varphi\sin\varphi\left(\mathrm{d}\varepsilon_1 - \frac{\mathrm{d}\varepsilon_2 + \mathrm{d}\varepsilon_3}{2} - \cos 2\theta\frac{\mathrm{d}\varepsilon_2 - \mathrm{d}\varepsilon_3}{2}\right)\vec{t}_1 + \cdots + \sin\varphi\cos\theta\sin\theta(\mathrm{d}\varepsilon_2 - \mathrm{d}\varepsilon_3)\vec{t}_2 \tag{C.1}$$

with $\vec{n} = \begin{bmatrix} \cos\varphi \\ \sin\varphi\cos\theta \\ \sin\varphi\sin\theta \end{bmatrix}, \vec{t}_1 = \begin{bmatrix} \sin\varphi \\ -\cos\varphi\cos\theta \\ -\cos\varphi\sin\theta \end{bmatrix}$ and $\vec{t}_2 = \vec{n}\wedge\vec{t}_1 = \begin{bmatrix} 0 \\ \sin\theta \\ -\cos\theta \end{bmatrix}$.

Over a strain probe test, vector $\mathrm{d}\vec{\varepsilon} = \begin{bmatrix} \mathrm{d}\varepsilon_1 \\ \mathrm{d}\varepsilon_2 \\ \mathrm{d}\varepsilon_3 \end{bmatrix}$ takes the form $\mathrm{d}\vec{\varepsilon} = \begin{bmatrix} \mathrm{d}e\cos\alpha_\varepsilon \\ \mathrm{d}e\sin\alpha_\varepsilon\cos\beta_\varepsilon \\ \mathrm{d}e\sin\alpha_\varepsilon\sin\beta_\varepsilon \end{bmatrix}$. Eq. (C.1) can therefore be rewritten as:

$$\frac{\mathrm{d}\widehat{\vec{u}}_t}{2r_g\mathrm{d}e} = \cos\varphi\sin\varphi\left(\cos\alpha_\varepsilon - \frac{\sqrt{2}}{2}\sin\alpha_\varepsilon\cos\left(\beta_\varepsilon - \frac{\pi}{4}\right) + \frac{\sqrt{2}}{2}\cos 2\theta\sin\alpha_\varepsilon\sin\left(\beta_\varepsilon - \frac{\pi}{4}\right)\right)\vec{t}_1 + \cdots$$
$$+ \frac{\sqrt{2}}{2}\sin\varphi\cos\theta\sin\theta\sin\alpha_\varepsilon\sin\left(\beta_\varepsilon - \frac{\pi}{4}\right)\vec{t}_2 \tag{C.2}$$

From the definition of angle α appearing in Fig. 3, Eq. (44) can finally be deduced:

$$\tan\alpha = \frac{\sin 2\theta \sin\alpha_\varepsilon \sin\left(\beta_\varepsilon - \frac{\pi}{4}\right)}{\cos\varphi\left(\sqrt{2}\cos\alpha_\varepsilon + \sin\alpha_\varepsilon \cos\left(\beta_\varepsilon - \frac{\pi}{4}\right) + \cos 2\theta \sin\alpha_\varepsilon \sin\left(\beta_\varepsilon - \frac{\pi}{4}\right)\right)}$$

References

Bardet, J.P., 1994. Observations on the effects of particle rotations on the failure of idealized granular materials. Mechanics of Materials 18, 159–182.

Balendran, B., Nemat-Nasser, S., 1993a. Double sliding model cyclic deformation of granular materials including dilatancy effects. Journal of the Mechanics and Physics of Solids 41 (3), 573–612.

Balendran, B., Nemat-Nasser, S., 1993b. Viscoplastic flow of planar granular materials. Mechanics of Materials 16, 1–12.

Bardet, J.P., Proubet, J., 1989. Application of micro-mechanics to incrementally nonlinear constitutive equations for granular media. In: Biarez, J., Gourvès, R. (Eds.), Powders and Grains, pp. 265–273.

Bardet, J.P., 1994a. Numerical simulations of the incremental responses of idealized granular materials. International Journal of Plasticity 10 (8), 879–908.

Bardet, J.P., 1994b. Observations on the effects of particle rotations on the failure of idealized granular materials. Mechanics of Materials 18, 159–182.

Bardet, J.P., 1998. Introduction to computational granular mechanics. In: Cambou, B. (Ed.), Behaviour of Granular Materials. Springer, Wien, New York, pp. 99–169.

Bazant, Z.P., 1978. Endochronic inelasticity and incremental plasticity. International Journal of Solids and Structures 14, 691–714.

Bazant, Z.P., Gambarova, P.G., 1984. Crack shear in concrete: crack band microplane model. ASCE Journal of Structural Engineering 110 (9), 2015–2035.

Bigoni, D., Hueckel, T., 1991. Uniqueness and localization, I. Associative and non-associative elastoplasticity. International Journal of Solids and Structures 28 (2), 197–213.

Caillerie, D., 1995. Evolution quasistatique d'un milieu granulaire, loi incrémentale par homogénéisation. In: Des matériaux aux Ouvrages. Hermès publ., pp. 53–80.

Calvetti, F., Combe, G., Lanier, J., 1997. Experimental micro-mechanical analysis of a 2D granular material, relation between structure evolution and loading path. Mechanics of Cohesive-Frictional Materials 2, 121–163.

Calvetti, F., Viggiani, C., Tamagnini, C., 2003. A numerical investigation of the incremental behavior of granular soils. Italian Geotechnical Journal (3), 11–29.

Cambou, B., 1993. From global to local variables in granular materials. In: Thorton (Ed.), Powders & Grains. Balkema, Rotterdam, pp. 73–86.

Cambou, B., Dubujet, P., Emeriault, F., Sidoroff, F., 1995. Homogenization for granular materials. European Journal of Mechanics, A/Solids 14 (2), 255–276.

Chang, C.S., 1992. Micromechanical modelling of deformation and failure for granulates with frictional contacts. Mechanics of Materials 16, 13–24.

Chang, C.S., Liao, C.L., 1994. Estimates of elastic modulus for media of randomly packed granulates. Applied Mechanics Review 47, 197–206.

Chang, C.S., Misra, A., Sundaram, S., 1990. Micro-mechanical modelling of cemented sands under low amplitude oscillations. Geotechnique 40 (2), 251–263.

Christoffersen, J., Mehrabadi, M.M., Nemat-Nasser, S., 1981. A micro-mechanical description of granular material behavior. Journal of Applied Mechanics 48, 339–344.

Cundall, P.A., Roger, D.H., 1992. Numerical modelling of discontinua. Engineering Computations 9, 101–113.

Cundall, P.A., Strack, O.D.L., 1979. A discrete numerical model for granular assemblies. Géotechnique 29, 47–65.

Dantu, P., 1957. Contribution à l'étude mécanique et géométrique des milieux pulvérulents. In: Proceedings of the 4th International Conference on Soil Mechanics and Foundation Engineering, vol. 1, p. 144.

Darve, F., 1990. The expression of rheological laws in incremental form and the main classes of constitutive equations. In: Darve, F. (Ed.), Geomaterials Constitutive Equations and Modelling. Taylor and Francis Books, pp. 123–148.

Darve, F., Labanieh, S., 1982. Incremental constitutive law for sands and clays, simulations of monotonic and cyclic tests. International Journal for Numerical and Analytical Methods in Geomechanics 6, 243–275.

Darve, F., Laouafa, F., 2000. Instabilities in granular materials and application to landslides. Mechanics of Cohesive-Frictional Materials 5 (8), 627–652.

Darve, F., Laouafa, F., 2002. Constitutive equations and instabilities of granular materials. In: Capriz et al. (Eds.), Modelling and Mechanics of Granular and Porous Materials. Birkhauser publ., pp. 3–43.
Darve, F., Roguiez, X., 1998. Homogeneous bifurcation in soils. In: Adachi et al. (Eds.), Bifurcation and Localization for Soils and Rocks. Balkema Publisher, pp. 43–50.
Darve, F., Vardoulakis, I., 2005. Instabilities and degradations in geomaterials. In: Darve, Vardoulakis (Eds.). Springer Publishers.
Darve, F., Flavigny, E., Meghachou, M., 1995. Yield surfaces and principle of superposition revisited by incrementally non-linear constitutive relations. International Journal of Plasticity 11 (8), 927–948.
Darve, F., Servant, G., Laouafa, F., Khoa, H.D.V., 2004. Failure in geomaterials, continuous and discrete analyses. Computer Methods in Applied Mechanics and Engineering 193, 3057–3085.
De Josselin de Jong, G., 1959. Statics and kinematics in the failable zone of granular material. Thesis, University of Delft.
De Josselin de Jong, G., 1971. The double sliding, free rotating model for granular assemblies. Géotechnique 21, 155–163.
Drescher, A., 1976. An experimental investigation of flow rules for granular materials using optically sensitive glass particles. Géotechnique 26, 591–601.
Drucker, D., 1951. A more fundamental approach to stress–strain relations. In: 1st US National Congress of Applied Mechanics, ASME, pp. 487–491.
Drucker, D., Prager, W., 1952. Soil mechanics and plastic analysis for limit design. Quarterly of Applied Mathematics 10, 157–165.
Field, W.G., 1963. Toward the statistical definition of a granular mass. In: Proceedings of 4th Austria–New Zealand Conference on Soil Mechanics and Foundation Engineering, pp. 143–148.
Gudehus, G., 1979. A comparison of some constitutive laws for soils under radially symmetric loading and unloading. In: Aachen, Wittke (Eds.), 3rd International Conference Numerical Methods in Geomechanics, 4. Balkema Publisher, pp. 1309–1324.
Hill, R., 1958. A general theory of uniqueness and stability in elastic–plastic solids. Journal of the Mechanics and Physics of Solids 6, 236–249.
Hill, R., 1965. Continuum micro-mechanics of elastoplastic polycrystals. Journal of the Mechanics and Physics of Solids 13, 89–101.
Hill, R., 1966. Generalized relations for incremental deformation of metal crystals by multislip. Journal of the Mechanics and Physics of Solids 14 (2), 95–102.
Hill, R., 1967a. On the classical constitutive relations for elastic–plastic solids. In: Broberg, B., Hult, J., Niordson, F. (Eds.), Recent Progress in Applied Mechanics. Folke Odqvist Volume. Almqvist and Wiksell, pp. 241–249.
Hill, R., 1967b. The essential structure of constitutive laws for metal composites and polycrystals. Journal of the Mechanics and Physics of Solids 15 (2), 79–95.
Hill, R., 1967c. Eigenmodal deformations in elastic–plastic continua. Journal of the Mechanics and Physics of Solids 15, 371–386.
Horne, M.R., 1965. The behaviour of an assembly of rotund, rigid cohesionless particles—I, II. Proceedings of the Royal Society of London 286, 62–97.
Jenkins, J.T., Strack, O.D.L., 1993. Mean-field inelastic behavior of random arrays of identical spheres. Mechanics of Materials 16, 25–33.
Kanatani, K.I., 1983. Mechanical properties of ideal granular materials. In: Jenkins, J.T., Satake, M. (Eds.), Mechanics of Granular Materials, New Models and Constitutive Relations. Elsevier, pp. 235–244.
Kanatani, K.I., 1984. Distribution of directional data and fabric tensors. International Journal of Engineering Sciences 22 (2), 149–164.
Kishino, Y., 1988. Disc model analysis of granular media. In: Satake, M., Jenkins, J.T. (Eds.), Micromechanics of Granular Materials, 2nd US–Japan Seminar on the Mechanics of Granular Materials. Elsevier, pp. 143–152.
Kishino, Y., 2003. On the incremental non-linearity observed in a numerical model for granular media. Italian Geotechnical Journal (3), 30–38.
Kolymbas, D., 1999. Introduction to Hypoplasticity. Balkema Publisher, 104 p.
Kolymbas, D., 1991. An outline of hypoplasticity. Archive of Applied Mechanics 61, 143–151.
Laouafa, F., Darve, F., 2002. Modelling of slope failure by a material instability mechanism. Computers and Geotechnics 24 (4), 301–325.
Love, A.E.H., 1927. A Treatise of Mathematical Theory of Elasticity. Cambridge University Press, Cambridge.
Luding, S., 2004. Micro–macrotransition for anisotropic, frictional granular packings. International Journal of Solids and Structures 41 (21), 5821–5836.
Mandel, J., 1966. Conditions de stabilité et Postulat de Drucker. In: Kravtechenko, Sirieys (Eds.), Rheology and Soil Mechanics. Springer-Verlag Publisher, pp. 58–68.
Mehrabadi, M.M., Cowin, S.C., 1978. Initial planar deformation of dilatant granular materials. Journal of the Mechanics and Physics of Solids 26, 269–284.
Mehrabadi, M.M., Oda, M., Nemat-Nasser, S., 1982. On statistical description of stress and fabric in granular materials. International Journal for Numerical and Analytical Methods in Geomechanics 6, 95–108.
Mehrabadi, M.M., Loret, B., Nemat-Nasser, S., 1993. Incremental constitutive relations for granular materials based on micromechanics. Proceedings of the Royal Society of London 441, 433–463.

Nemat-Nasser, S., 2000. A micromechanically-based constitutive model for frictional deformation of granular materials. Journal of the Mechanics and Physics of Solids 48 (6–7), 1541–1563.

Nemat-Nasser, S., Mehrabadi, M.M., 1983. Stress and fabric in granular masses. In: Jenkins, J.T., Satake, M. (Eds.), Mechanics of Granular Materials, New Models and Constitutive Relations. Elsevier Science Publishers, pp. 1–8.

Nemat-Nasser, S., Mehrabadi, M.M., 1984. Micromechanically based rate constitutive descriptions for granular materials. In: Desai, C.S., Gallagher, R.H. (Eds.), Mechanics of Engineering Materials, Proceedings of the International Conference on Constitutive Law for Engineering Mat. Theory and Application. John Wiley & Sons, New York.

Nemat-Nasser, S., Zhang, J., 2002. Constitutive relations for cohesionless frictional granular materials. International Journal of Plasticity, 531–547.

Nemat-Nasser, S., Mehrabadi, M.M., Iwakuma, T., 1981. On certain macroscopic and microscopic aspects of plastic flow of ductile materials. In: Nemat-Nasser, S. (Ed.), Three-Dimensional Constitutive Relations and Ductile Fracture. North Holland, pp. 157–172.

Nicot, F., 2003a. Modélisation multi-échelles des géomatériaux, contribution au traitement des risques naturels. Habilitation à Diriger des Recherches, Institut National polytechnique de Grenoble.

Nicot, F., 2003b. Constitutive modelling of a snowcover with a change in scale. European Journal of Mechanics A/Solids 22–23, 325–340.

Nicot, F., 2004. From a constitutive modelling of a snowcover to the design of flexible structures. Part I, Mechanical modelling. International Journal of Solids and Structures 41 (11–12), 3317–3337.

Nicot, F., Darve, F., 2004. Multiscale modeling of geomaterials. In: Pande, Pietruszczak (Eds.), Numerical Models in Geomechanics, NUMOG IX. Taylor and Francis Group, pp. 11–16.

Nicot, F., Darve, F., 2005. A multiscale approach to granular materials. Mechanics of Materials 37 (9), 980–1006.

Nova, R., 1994. Controllability of the incremental response of soil specimens subjected to arbitrary loading programs. Journal of Mechanical Behavior of Materials 5 (2), 193–201.

Oda, M., Konishi, J., 1974. Microscopic deformation mechanism of granular material in simple shear. Soils and Foundations 14 (4), 15–32.

Oda, M., Konishi, J., Nemat-Nasser, S., 1980. Some experimentally based fundamental results on the mechanical behaviour of granular materials. Géotechnique 30 (4), 479–495.

Oda, M., Konishi, J., Nemat-Nasser, S., 1982. Experimental evaluation of strength of granular materials, effects of particle rolling. Mechanics of Materials 1, 269–283.

Oda, M., Iwashita, K., Kakiuchi, T., 1997. Importance of particle rotation in the mechanics of granular materials. In: Behringer, Jenkins (Eds.), Powders and Grains. Balkema, pp. 207–210.

Pastor, M., Zienkiewicz, O.C., Chan, A.H.C., 1990. Generalized plasticity and the modeling on soil behavior. Int. Journal for Numerical and Analytical Methods in Geomechanics 14, 151–190.

Radjai, F., Wolf, D., Jean, M., Moreau, J.J., 1998. Bimodal character of stress transmission in granular packing. Physical Review Letters 80 (1), 61–64.

Radjai, F., Roux, S., Moreau, J.J., 1999. Contact forces in a granular packing. Chaos 9 (3), 544–550.

Rice, J.R., 1970. On the structure of stress–strain relations for time-dependent plastic deformation in metals. Journal of Applied Mechanics 37, 728–737.

Rice, J.R., 1975. Continuum mechanics and thermodynamics of plasticity in relation to microscale deformation mechanisms. In: Argon, A.S. (Ed.), Constitutive Equations in Plasticity. MIT Press, Cambridge, pp. 23–79.

Rothenburg, L., Kruyt, N.P., 2004. Critical state and evolution of coordination number in simulated granular materials. International Journal of Solids and Structures 41 (21), 5763–5774.

Satake, M., 1978. Constitution of mechanics of granular materials through graph representationTheoretical and Applied Mechanics, vol. 26. University of Tokyo Press, pp. 257–266.

Satake, M., 1982. Fabric tensor in granular materials. In: IUTAM Conference on Deformation and Failure of Granular Materials, Delft, pp. 63–68.

Spencer, A.J.M., 1964. A theory of the kinematics of ideal soils under plane strain conditions. Journal of the Mechanics and Physics of Solids 12, 337–351.

Taylor, G.I., 1934. The mechanism of plastic deformation of crystals—I, theoretical. Proceedings of the Royal Society of London, A 145, 362–387.

Taylor, G.I., 1938. Plastic strains in metals. Journal of the Institute of Metals 62, 307–325.

Tordesillas, A., Walsh, D.C., 2002. Incorporating rolling resistance and contact anisotropy in micromechanical models of granular media. Powder Technology 124, 106–111.

Weber, J., 1966. Recherches concernant les contraintes intergranulaires dans les milieux pulvérulents. Bulletin de Liaison des Ponts-et-Chaussées (20), 1–20.

Yanagisawa, E., 1983. Influence of void ratio and stress condition on the dynamic shear modulus of granular media. In: Shahinpoor (Ed.), Advances in the Mechanics and the Flow of Granular Materials. Gulf Publishing, Houston, pp. 947–960.

Zienkiewicz, O.C., Pande, G.N., 1977. Time dependent multilaminate model of rocks, a numerical study of deformation and failure of rock masses. International Journal for Numerical and Analytical Methods in Geomechanics 1, 219–247.

Zienkiewicz, O.C., Mroz, Z., 1984. Generalized plasticity formulation and applications to geomechanics. In: Desai, C.S., Gallagher, R.H. (Eds.), Mechanics of Engineering Materials. Wiley, pp. 655–679.